LETTERS
https://doi.org/10.1038/s41587-021-00878-8

nature biotechnology

Check for updates

Engineering luminescent biosensors for point-of-care SARS-CoV-2 antibody detection

Susanna K. Elledge[1,9], Xin X. Zhou[1,9], James R. Byrnes[1], Alexander J. Martinko[2], Irene Lui[1], Katarina Pance[1], Shion A. Lim[1], Jeff E. Glasgow[1], Anum A. Glasgow[3], Keirstinne Turcios[4], Nikita S. Iyer[4], Leonel Torres[4,5], Michael J. Peluso[5], Timothy J. Henrich[4], Taia T. Wang[6,7], Cristina M. Tato[6], Kevin K. Leung[1], Bryan Greenhouse[4,5] and James A. Wells[1,6,8] ✉

Current serology tests for severe acute respiratory syndrome coronavirus 2 (SARS-CoV-2) antibodies mainly take the form of enzyme-linked immunosorbent assays, chemiluminescent microparticle immunoassays or lateral flow assays, which are either laborious, expensive or lacking sufficient sensitivity and scalability. Here we present the development and validation of a rapid, low-cost, solution-based assay to detect antibodies in serum, plasma, whole blood and to a lesser extent saliva, using rationally designed split luciferase antibody biosensors. This new assay, which generates quantitative results in 30 min, substantially reduces the complexity and improves the scalability of coronavirus disease 2019 (COVID-19) antibody tests. This assay is well-suited for point-of-care, broad population testing, and applications in low-resource settings, for monitoring host humoral responses to vaccination or viral infection.

As the vaccine deployment starts worldwide for COVID-19, broad antibody testing for SARS-CoV-2 faces severe limitations. Although nucleic acid testing is critical to detecting the virus, serological antibody tests are vital tools for monitoring the dynamic human humoral response to SARS-CoV-2 vaccination and viral infection[1]. Population-scale, longitudinal evaluation of antibody responses is needed to determine the strength and duration of immunity to the primary virus, to the variants, and to vaccines, which is important in informing public policy and vaccination strategies[2–7]. In addition, antibody tests serve as a complement or an alternative to nucleic acid diagnostics for patients with a low viral load or for low-resource areas where expensive reverse transcription polymerase chain reaction (RT–PCR) testing is difficult to access[8–10]. Serological tests also support therapeutic development through identification of either individuals who could serve as donors for convalescent serum therapeutics[11], or patients with potentially strong neutralizing antibodies that can be produced in vitro as new antivirals and prophylactics[12,13]. All these applications would be greatly accelerated with an assay that is simple, rapid and high throughput, without sacrificing accuracy and sensitivity.

Traditional serological assays are not optimal in the face of this broad pandemic. The most widely used laboratory serological tests take the form of enzyme-linked immunosorbent assays (ELISAs)[3,14–16], which usually entail a more than 2-h protocol involving several steps of protein incubation and washes and is not readily amenable to deployment outside of a laboratory. A faster but considerably more expensive approach is a lateral flow assay[17,18]. However, lateral flow assays can produce less reliable results depending on the quality of the lateral flow device and different evaluation criteria[18,19]. In addition, lateral flow tests poorly capture the magnitude of a patient's antibody response, as the test is qualitative and not quantitative. An alternative is a chemiluminescent microparticle immunoassay (for example, the Abbott AdviseDx and Roche Elecsys SARS-CoV-2 tests), but these assays are expensive, lacking scalability, and typically require specific integrated instrument platforms to perform the tests.

Here we describe a next-generation, simple and rapid assay to meet the mounting needs for broad antibody testing in the face of the ongoing pandemic and the population-wide vaccine deployment. The assay, which is compatible with serum, plasma, whole blood and saliva samples, uses a simple split luciferase (spLUC) antibody sensor to generate quantitative serological data in 30 min. Testing of over 150 patient serum/plasma samples across three validation cohorts demonstrates that the spLUC assay has a sensitivity of 89% for detecting anti-S protein antibodies and 98% for detecting anti-N protein antibodies and a specificity of over 99% for both.

Engineering spLUC biosensors for SARS-CoV-2 antibody detection

When envisioning a next-generation serological assay, we hypothesized that sensitive biosensors for anti-SARS-CoV-2 antibodies could be used to greatly enhance the speed and simplicity of serological testing[20]. We constructed anti-SARS-CoV-2 antibody biosensors by fusing split nanoluciferase (NanoLuc) fragments SmBiT and LgBiT[20] to SARS-CoV-2 viral protein antigens (Fig. 1a). Because an antibody has two fragment antigen-binding (Fab) arms, incubating serum with 1:1 mixed SmBiT and LgBiT biosensors will result in half of the antiviral antibodies binding LgBiT with one Fab arm and SmBiT with the other Fab arm. This hetero-bivalent interaction localizes the LgBiT and SmBiT fragments in close proximity, resulting in reconstitution of an intact, active NanoLuc enzyme for luminescence-based detection of reactive antibodies.

[1]Department of Pharmaceutical Chemistry, University of California, San Francisco, San Francisco, CA, USA. [2]Soteria Biotherapeutics, San Francisco, CA, USA. [3]Department of Bioengineering and Therapeutic Sciences, University of California, San Francisco, San Francisco, CA, USA. [4]Division of Experimental Medicine, University of California, San Francisco, San Francisco CA, USA. [5]Division of HIV, Infectious Diseases, and Global Medicine, University of California, San Francisco, San Francisco, CA, USA. [6]Chan Zuckerberg Biohub, San Francisco, CA, USA. [7]Departments of Medicine and of Microbiology and Immunology, Stanford University School of Medicine, Stanford, CA, USA. [8]Department of Cellular and Molecular Pharmacology, University of California, San Francisco, San Francisco, CA, USA. [9]These authors contributed equally: Susanna K. Elledge, Xin X. Zhou. ✉e-mail: jim.wells@ucsf.edu

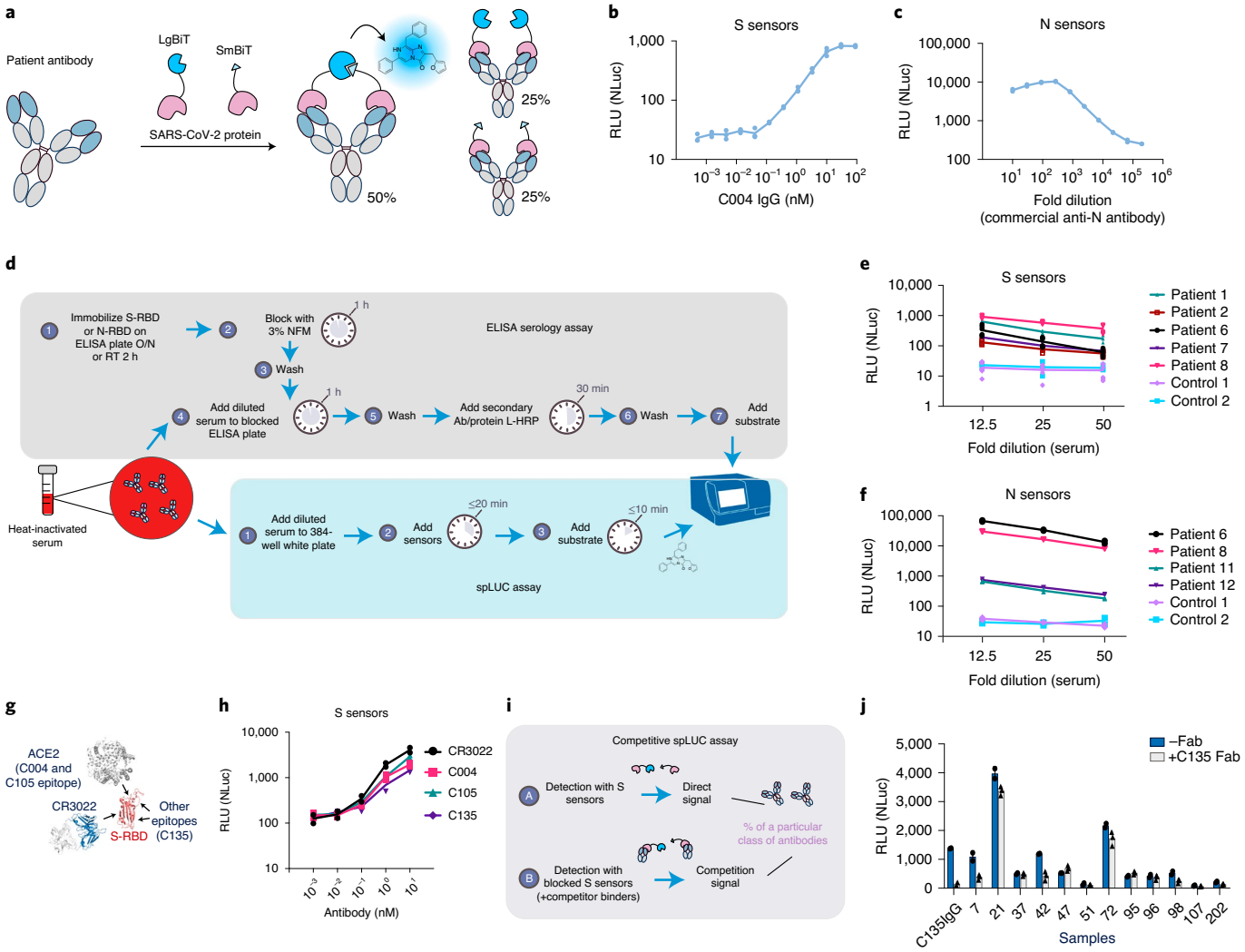

Fig. 1 | Engineering luminescent biosensors for rapid and quantitative detection of SARS-CoV-2 antibodies. a, Schematic of the solution-based serology assay. Patient antibodies are incubated with SARS-CoV-2 S or N proteins fused to LgBiT/SmBiT. For the population of antibodies with one arm bound to the LgBiT sensor and the other arm bound to the SmBiT sensor, the NanoBiT luciferase enzyme is reconstituted and, thus, can produce active luciferase signal. **b**, Dose-dependent spLUC signals for the recombinant anti-S-RBD antibody C004 in PBST + 10% FBS. Two technical replicates are plotted from $n = 1$ independent experiment. **c**, Dose-dependent spLUC signals for an anti-N-RBD antibody (Sino Biological, cat. no. 40588-T62-50) in PBST + 8% FBS. Two technical replicates are plotted from $n = 1$ independent experiment. **d**, Comparison of assay procedures between the ELISA and the spLUC assay. While ELISA takes more than 2 h and involves multiple wash and incubation steps, the spLUC solution-based assay is simply completed in 30 min or less without the need for wash steps. **e**, The S (L15 + S25) sensors are able to detect antibodies in 5/5 recovered patients with COVID-19. At all dilutions tested, all five patients generated signal above the background signal of two control serum samples collected before the pandemic. Each dot represents a technical replicate. $n = 2$ independent experiments with three replicates each are plotted for all samples, except for those of Patient 1, Patient 7 and Control 2, which have $n = 1$ independent experiment plotted owing to limited reagents. **f**, The N (LC + SC) sensors are able to detect antibodies in 4/4 recovered patients with COVID-19. At all dilutions of serum tested, all four patients generated signal above the background signal of two control serum samples collected before the pandemic. Two technical replicates are plotted from $n = 1$ independent experiment. **g**, Patient antibodies for SARS-CoV-2 have various epitopes on the S-RBD (red). C004 and C105 have ACE2-competitive epitopes, whereas C135 and CR3022 (blue) have non-ACE2-competitive epitopes. **h**, S sensors can detect patient antibodies of various epitopes with similar sensitivity. C004, C105, C135 and CR3022 patient antibodies were incubated with the S sensors at ten-fold antibody dilutions from 10 nM to 0.001 nM. The average of three technical replicates from $n = 2$ independent experiments are plotted. **i**, Schematic of antibody epitope competition assay with patient serum samples. Direct signal is compared to signal generated in the presence of the pre-incubated 1 μM Fab +1 nM sensor. **j**, Competition assay performed with C135 Fab on 12 outpatient sera samples and recombinant C135 IgG protein. Samples were incubated with either no Fab (blue) or C135 Fab (off-white). Sera 7, 42 and 98 showed more than 50% decreases in luminescence signal, suggesting the presence of antibodies with the C135 epitope. Each dot represents a technical replicate from $n = 1$ independent experiment. The center of the bar represents the mean of the measurements. Direct signals (−Fab) were measured in technical duplicates, and competition signals (+C135 Fab) samples were done in technical triplicate. For **b**, **c**, **e**, **f** and **h**, the center of the line represents the mean of all measurements. Lines connecting the means of the samples are plotted. RLU, relative luminescence unit; RT, room temperature; NFM, non-fat milk; O/N, overnight.

We chose to develop S and N sensors for SARS-CoV-2 antibody tests because COVID-19 patient antibodies are predominantly directed against epitopes on the viral S protein, which interacts with the host receptor angiotensin-converting enzyme 2 (ACE2) and mediates viral entry[21], and the N protein, which packages the viral genome into a ribonucleocapsid[22]. These two viral

proteins are the primary antigens used in the current COVID-19 serological tests[3,14,23–26].

The S sensors were constructed by fusing NanoLuc fragments to its receptor-binding domain (S-RBD), which is the primary target of neutralizing antibodies (Extended Data Fig. 1a,b)[3,14,26,27]. We modeled S-RBD binding to two antibodies—C105 (refs. [12,28]), an ACE2-competitive binder, and CR3022 (ref. [29]), an ACE2 non-competitive binder—to determine linker lengths (Supplementary Text and Extended Data Fig. 1c,d). Based on the models, we constructed SmBiT fusions to the S-RBD C terminus with 15 or 25 residue glycine/serine (GS) linkers (S15 and S25) and LgBiT fusions to S-RBD C terminus with 5, 15 or 25 residue GS linkers (L5, L15 and L25). These variants varied in expression yields (Extended Data Fig. 1e). Using recombinantly expressed S-RBD antibodies and ACE2 variants[30], we determined the optimal linker variant, enzyme concentration, buffer conditions and effect of antibody–antigen binding affinity to signal strength (Supplemental Text, Extended Data Figs. 1 and 2 and Supplementary Fig. 1). The (L15 + S25) sensor pair at 1 nM enzyme concentration was identified as optimal, and these conditions were used for all subsequent assays.

In further characterizing the relationship between assay signal strength and antibody concentration/binding affinity, we performed ordinary differential equation modeling in R (Supplemental Text and Extended Data Fig. 3). The modeling predicted a linear relationship between antibody concentration and luciferase signal (Extended Data Fig. 3b), consistent with our experimental data (Fig. 1b). In addition, the results highlighted that the sensors at 1 nM are more sensitive to an antibody binder with a $K_D \leq 1$ nM (Extended Data Fig. 3b,c). This threshold is equivalent to the median affinity reported for polyclonal antibody repertoires[31,32].

To construct the N sensors, we used the N-terminal sequence because amino acids (aa) 44–257 are found to be more immunogenic than the C-terminal dimerization domain (aa 258–419) (Extended Data Fig. 4a)[33]. In addition, dimerization promoted by the C-terminal domain might lead to high basal NanoLuc reconstitution levels. The atomic structures of $N_{44–180}$[22] showed that the N and C termini are not in close proximity, and, therefore, fusion at the N or C terminus might result in different sensor sensitivity (Extended Data Fig. 4b). Given this knowledge, three fusion sensor pairs were designed: (1) LN + SN: L/S–$N_{44–257}$; (2) LC + SC: $N_{44–180}$–L/S; and (3) LC2 + SC2: $N_{44–257}$–L/S, where L and S represent LgBiT and SmBiT, respectively, C represents C-terminal fusion and N represents N-terminal fusion (Extended Data Fig. 4c). Testing on a commercial polyclonal anti-N protein antibody revealed that the LC + SC and LC2 + SC2 sensors generated stronger signals over LN + SN (Extended Data Fig. 4d). The LC + SC sensors generated linear, dose-dependent signals with commercial anti-N protein antibody (Fig. 1c).

We next designed a simple and rapid protocol to assay a pilot set of serum samples from convalescent patients with SARS-CoV-2 (Fig. 1d). Two healthy control sera collected before the emergence of the SARS-CoV-2 virus were also tested. Serial dilutions (1:12.5, 1:25 and 1:50) of heat-inactivated sera were measured using S or N sensors. Robust, dose-dependent luminescence signal was observed across all serum concentrations tested, with the 12.5-fold dilution showing the highest signal (Fig. 1e,f). The S (L15 + S25) sensors generated signal for all five patients tested (Fig. 1e). The N (LC + SC) sensors detected patient antibodies from all four patients tested (Fig. 1f). However, the N (LN + SN) sensors detected antibodies from only two patient sera samples that had the strongest seropositivity (Extended Data Fig. 4e), which further confirmed that a C-terminal fusion enhances NanoLuc reconstitution relative to the N-terminal fusion. Interestingly, much higher signals were generated with the N (LC + SC) sensor compared to the S sensor. This could be due to differing levels of anti-N or S antibodies in the patients[34], the affinity of antibodies, or a favored geometry for split enzyme reconstitution when anti-N antibodies bind to the N (LC + SC) sensors.

Competitive spLUC assay to profile epitope classes of antibodies

In addition to a test to determine total binding antibodies, an assay that allows profiling of epitope classes of antibodies can be

Fig. 2 | Characterization of outpatient and inpatient serum samples using the spLUC test. Cohort 1: samples drawn during the convalescent phase of an outpatient group; Cohort 2: samples drawn during the acute phase or the convalescent phase of a hospitalized group; and Cohort 3: samples drawn during the convalescent phase of a mixed inpatient and outpatient group. A 10-base logarithmic scale conversion was applied to all the solution assay signals for the correlation analysis, unless otherwise specified. **a**, SpLUC assay tested on expanded COVID-19 patient cohorts with S sensors at 1:12.5 serum dilution. Dots represent the average between two technical duplicates. Lines represent median values. The inpatient samples showed significantly higher antibody titers than the outpatient cohorts. Sample sizes are as indicated in parentheses: Control (56), Cohort 1 (57), Cohort 2 (55), Cohort 3 outpatient (47) and Cohort 3 inpatient (9). **b**, SpLUC assay tested on expanded COVID-19 patient cohorts with N sensors at 1:12.5 serum dilution. The inpatient samples showed significantly higher antibody titers than the outpatient cohorts. Sample sizes are as indicated in parentheses: Control (120), Cohort 1 (56), Cohort 2 (47), Cohort 3 outpatient (47) and Cohort 3 inpatient (9). **c**, A positive correlation ($R = 0.78$) was observed between S sensor signal and N sensor signal in the three cohort samples. All cohorts individually presented a similar trend (Extended Data Fig. 5). The line represents linear regression. In total, 159 patient samples are plotted. **d**, Correlation of spLUC signals (Cohort 1) to neutralization efficiency[12]. S sensor signal (blue) and N sensor signal (purple) are plotted against 50% maximal neutralization titer (NT_{50}). Both show positive correlation ($R = 0.76$ for S and NT_{50} and $R = 0.62$ for N and NT_{50}). Fifty-seven patient samples are plotted for the S sensor, and 56 samples are plotted for the N sensor. **e**, Inpatients show significantly higher signal than outpatients in all three cohorts ($P < 0.0001$). Sample sizes are as indicated in parentheses: S-outpatient (104), S-inpatient (64), N-outpatient (103) and N-inpatient (56). **f**, Patients from Cohort 1 who reported higher disease severity (6–10 versus 1–5) had higher antibody titer for both S and N sensors, and the difference for N sensors is statistically significant ($P = 0.0049$). Sample sizes are as indicated in parentheses: S-score 1–5 (24), S-score 6–9 (33), N-score 1–5 (24) and N-score 6–9 (32). **g**, Higher overall antibody titers were observed in patients who reported fever compared to no-fever patients for Cohort 3. This difference was statistically significant for the S sensors ($P = 0.0011$) but not for the N sensors. Seventeen patient samples associated with no fever and 38 patient samples associated with a fever are plotted. **h**, Slightly higher overall antibody titers were observed in females than in males for Cohort 3, although the differences were not statistically significant. There is a similar trend for Cohort 1 (Supplementary Fig. 3a). The difference was more obvious for S sensors. Twenty-five female patient samples and 30 male patient samples are plotted. **i**, For Cohort 3, there is a slightly higher level of antibodies in the 60–85 age group compared to 19–39 and 40–59. There is a similar trend for Cohort 1 (Supplementary Fig. 3b). The differences were not statistically significant. Sample sizes are as indicated in parentheses: age 19–39 (23), age 40–59 (25) and age 60–85 (8). For **a** and **b**, *P* values (two-tailed) of a Kruskal–Wallis test with Dunn's multiple comparison post hoc testing to compare each clinical cohort with the healthy control group are indicated. For **c** and **d**, *R* values and *P* values (two-tailed) of a non-parametric Spearman correlation analysis are labeled in the graphs. For **e**–**i**, an unpaired Mann–Whitney test is performed, and *P* values (two-tailed) for each comparison are labeled on top of the datasets. For all panels, dots represent the average of two technical replicates from $n = 1$ independent experiment. For **a** and **b** and **e**–**i**, horizonal lines represent median values. For **c** and **d**, lines represent linear regression. RLU, relative luminescence unit.

highly valuable. In this regard, competitive ELISA assays developed by us and others have enabled characterization of percentage of ACE2-competitive antibodies[26,35]. However, S-RBD is known to have multiple additional neutralization epitopes outside of the ACE2-binding site. An assay that allows rapid, unbiased profiling of those alternative epitopes could unveil further details of a patient's humoral response to neutralize SARS-CoV-2.

We first showed that the spLUC assay can detect antibodies binding to various S-RBD epitopes (Fig. 1g). We expressed and tested four reported neutralizing antibodies against S-RBD. This includes C004 and C105 (ref. [12]), which are ACE2-competitive binders; CR3022 (ref. [29]), which binds at a cryptic site outside of the ACE2-binding site; and C135 (ref. [12]), which does not compete with C004, C105, CR3022 or ACE2-Fc, representing a third binding epitope on S-RBD (Supplementary Fig. 2). All four IgG antibodies generated dose-dependent luminescence signals at ≥0.1 nM concentrations (Fig. 1h).

We then designed a competitive spLUC assay to determine thepresence of a specific epitope class of antibodies (Fig. 1i). Of the four antibodies tested, C135 represents an unconventional and less understood epitope class. It neutralizes very potently (IC_{50} = 17 ng ml^{-1}) and might be used in combination with other ACE2-competitive binders as a cocktail therapy[12]. We converted C135 IgG to a single binding arm Fab binder and pre-incubated 1 μM of C135 Fab with the S sensors to generate 'blocked sensors'. We then determined how much signal from a patient's sample corresponds to antibodies with a C135 epitope by comparing signals between the original and the 'epitope-masked' sensors (Fig. 1i). We assayed 12 patient serum samples with representative high, medium and low anti-S-RBD antibody levels at a 1:25 dilution of serum. IgG C135 served as a control for competition with Fab C135. As expected, the luminescence signal of IgG C135 was reduced by ~90% with the blocked sensors. Sera 7, 42 and 98 showed more than 50% decreases in luminescence signals, indicating that a large portion of the antibodies in these samples are C135 competitive (Fig. 1j). These results suggest that antibodies recognizing this unconventional, neutralizing S-RBD epitope are present in a substantial proportion of patient samples. Performing this competitive spLUC assay with different competitive Fab antibodies in an expanded patient cohort could further understanding of the distribution of epitopes on S-RBD and the correlation between epitopes and clinical outcomes.

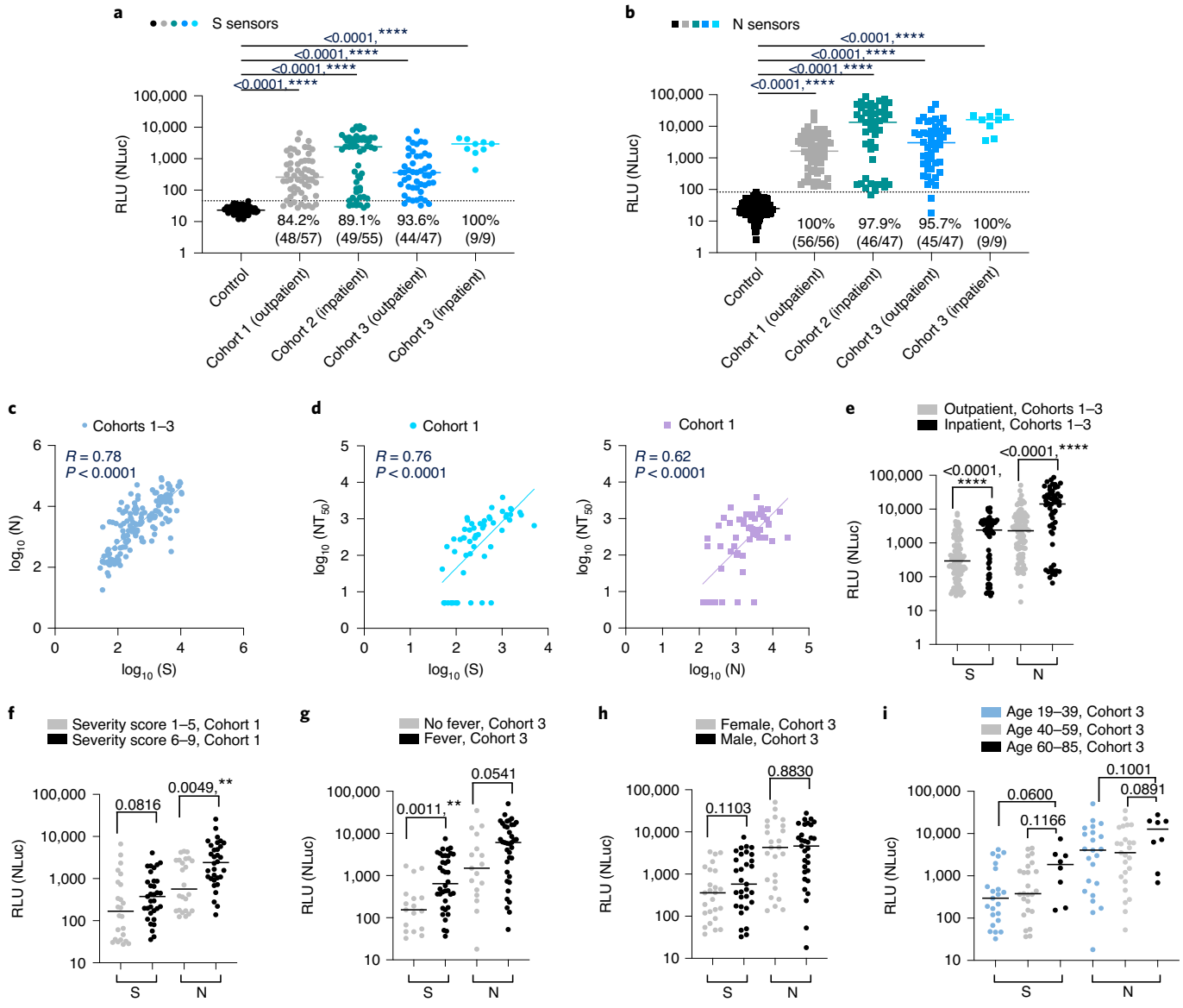

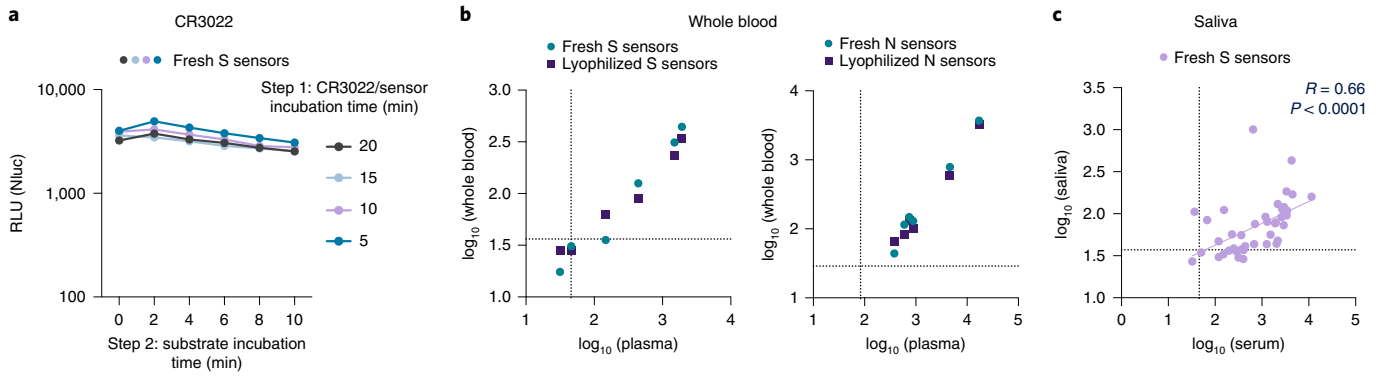

Fig. 3 | Adapting the assay for whole blood and saliva sample types. a, spLUC assays can be accomplished in as few as 5 min. CR3022 (10 nM) was incubated with S sensors for 5, 10, 15 or 20 min. Luciferase substrates were then added and incubated with the reaction mix for 0, 2, 4, 6, 8 or 10 min. All reactions showed bright luminescence signal. Each dot represents the average of two technical duplicates from $n = 1$ independent experiment. Lines connecting the means of the samples are plotted. **b**, The spLUC assay is compatible with whole blood samples and shows similar signal in the corresponding plasma samples with both fresh and lyophilized sensors. Each dot represents the average of two technical replicates from $n = 1$ independent experiment. A non-parametric Spearman correlation analysis was performed, and $R = 0.94$ was observed for S sensors, and $R = 1$ and 0.98 were observed for N sensor fresh and lyophilized sensors, respectively. **c**, Anti-S antibodies were detected in saliva samples with moderate sensitivity (33/42, 79%). The signals from saliva samples positively correlated with corresponding serum samples. Each dot represents the average of two technical replicates from $n = 1$ independent experiment. A non-parametric Spearman correlation analysis was performed, and the R value (0.66) and P value (<0.0001, two-tailed) are labeled in the graphs. The line represents linear regression.

Characterization of larger cohorts of serum/plasma samples using the spLUC assay

We next applied the spLUC assay in an expanded number of patients (Fig. 2). First, to determine assay cutoff values and specificity, which reflects how well an assay performs in a group of disease-negative individuals, we performed the tests on three cohorts of negative control samples (total $n = 144$), which included mainly healthy individual samples, 12 seasonal coronavirus patient samples and 20 flu vaccine pre- and post-vaccination samples. All controls were collected before the SARS-CoV-2 pandemic. These controls generated significantly lower luminescent signals than the COVID-19 patient sera samples (Fig. 2a,b). The range, median, mean and standard deviation values were calculated, and stringent cutoff values were determined by calculating the mean plus three standard deviations (Supplementary Table 1). With these determined cutoffs, we calculated the specificity of the S sensors (1:12.5 serum dilution) to be 100% (56/56) and the N sensors (1:12.5 serum dilution) to be 99.2% (119/120).

We then used the spLUC assay to study three additional cohorts of patient samples (Fig. 2a,b). Cohort 1 is an outpatient cohort recruited at the Rockefeller University Hospital[12]. The samples were collected from individuals free of COVID-19 symptoms for ≥14 d. The S sensors showed 84.2% (48/57) sensitivity, and the N sensors showed 100% (56/56) sensitivity. Cohort 2 samples consisted of remnant sera from patients with COVID-19 at Kaiser Permanente Hospitals of Northern California. These samples were drawn in any phase of infection, including the early acute phase. A subset of these patients, who might have not fully seroconverted at the time of sampling, had lower S sensor or N sensor signals than others in the spLUC assays. The sensitivities of the assays were 89% (49/55) for S sensors and 98% (46/47) for N sensors. Cohort 3 patients were part of the LIINC (Long-term Impact of Infection with Novel Coronavirus) study from San Francisco General Hospital and included plasma of a mixture of outpatient and inpatient samples drawn in the convalescent phase of the disease. With the S sensors, we detected antibodies in 94% (44/47) of outpatient samples and 100% (9/9) of inpatient samples. With the N sensors, we detected antibodies in 96% (45/47) of outpatient samples and 100% (9/9) of inpatient samples. For all cohorts, the S and N signals show a strong correlation (Fig. 2c and Extended Data Fig. 5). Consistent with previous findings, we observed varying degrees of anti-S and N antibody seropositivity among patients (Fig. 2a,b), which reflects a wide range of patient humoral response to this virus[8,2].

Notably, we observed strong correlation of spLUC assay results to anti-Fab and anti-IgG S-RBD ELISA signals (Extended Data Fig. 6a–c; $R = 0.43$–0.91). A base-10 logarithmic scale conversion was applied to the spLUC assay signals for the correlation analysis to ELISA signals. This non-linear correlation between the spLUC and ELISA assays is likely due to signal compression in ELISAs at high antibody concentrations (Abcam, ELISA guide). For all cohorts, the S sensor seronegative samples also had very low signals in S-RBD ELISA assays (Extended Data Fig. 6d–f), which confirmed the presence of low levels of anti-S-RBD antibodies in these sub-cohorts of patients. Interestingly, the correlations to IgM signals were much weaker (Extended Data Fig. 6a,b). It is possible that IgM was not sensitively detected by the spLUC assay owing to the weaker affinities of the individual binding arms in IgMs[36] or that the IgG response dominated the signal in many of the tested patients.

One of the key uses of a highly sensitive serology assay is to grade the quality of convalescent sera to neutralize virus[1]. In Cohort 1, our analysis showed that the S sensor signals correlated with the half-maximal neutralizing titers reported by Robbiani et al. (Fig. 2d, left panel), consistent with previous studies[4,12,14,37]. Moreover, we found that the N sensor signals showed a similar correlation with half-maximal neutralizing titer (Fig. 2d, right panel). Our results indicate that determining either anti-S or anti-N seropositivity is a general means to assess the neutralization potential of sera samples.

We further analyzed our data in the context of demographic and clinical features. First, the degree of seropositivity for inpatient samples was significantly higher than that of outpatient samples (Fig. 2a,b,e). Disease severity scores and fever were also associated with a stronger antibody response (Fig. 2f,g). These results indicated a direct correlation of disease severity and adaptive immune response, consistent with previous studies[2,4,8,10,12,38,39]. In addition, no statistical differences were observed in antibody titers between males and females (Fig. 2h and Supplementary Fig. 3a) or for different age groups (Fig. 2i and Supplementary Fig. 3b). We expect that analyzing a larger number of samples can further unveil if infected older adults develop more antibodies than younger individuals, as suggested in previous studies[18,19]. These results highlight

that clinical features are correlated with the antibody response of patients with COVID-19.

Collectively, our assay showed high sensitivity and specificity for all three representative cohorts of serum/plasma samples (including inpatient, outpatient, acute phase and convalescent phase samples), with an overall specificity of 100% (S sensor) and 99% (N sensor) and sensitivity of 89% (S sensor) and 98% (N sensor). These values are similar or superior to reported values for laboratory ELISA and lateral flow tests[18,19].

Additionally, we sought to determine the inter-day and intra-day assay variability. To further reduce labor work, we used a liquid handler system to dispense plasma, sensors and substrate. We characterized a set of 46 convalescent plasma samples multiple times over 2 d to determine assay variation (Extended Data Fig. 7a). We observed average intra-assay coefficient of variations (CVs) of 6% for both S and N sensors, intra-day CVs of 7% for S sensors and 9% for N sensors and inter-day CVs of 8% for S sensors and 9% for N sensors (Extended Data Fig. 7b).

The simplicity of the assay can greatly improve laboratory antibody test throughput. From our experience, one individual can run four plates of 96 samples (in total, 384 assays) per hour by hand with multi-channel pipettes. The automation of the assay is also straightforward as no wash step is involved. We showed that individual steps can be assisted with liquid dispenser instruments (Extended Data Fig. 7a). We further set up a workflow for full automation of this assay using the University of California, San Francisco (UCSF) Antibiome Center robotics platform (Extended Data Fig. 8a,b)[40], which will further improve assay throughput. A simulated run for 40 plates (3,840 assays) was estimated to take 3 h (Extended Data Fig. 8c). This robotic platform opens up the opportunity for characterizing hundreds of thousands of samples for population-wide epidemiology and longitudinal studies.

Adapting the assay for low-resource settings and expanded sample types

Lastly, we adapted our assays to begin to meet the clinical needs in remote and low-resources settings and for point-of-care deployment. A target assay profile was created based on a World Health Organization consensus meeting report on high-priority target product profiles for new tuberculosis diagnostics (Supplementary Table 2)[41]. Although the current properties of the assay meet most of the assay profile requirements, we tested to see if the reaction time (30 min), reagent format (frozen aliquots of sensors), luminescence instrument type (plate-based luminometer) and sample type (serum/plasma) could be further optimized.

We first tested if our initial reaction times (20-min sensor incubation and 10-min substrate incubation; Fig. 1d) are necessary and optimal. CR3022 (10 nM) was incubated with 1 nM S sensors for 5, 10, 15 and 20 min, followed by luciferase substrate addition and incubation for 0, 2, 4, 6, 8 and 10 min (Fig. 3a). We found that all time points resulted in similar, bright luminescence signal, suggesting that the time of the assay protocol can be further shortened.

We then tested if the sensors can be lyophilized for ambient temperature storage and transportation. Although a small quantity (0–30%) of S sensors and N sensors were lost due to the lyophilization process (Extended Data Fig. 9a), both the lyophilized S and the N sensors can still robustly detect recombinant IgG or patient antibodies in serum with similar sensitivities seen for the fresh sensors (Extended Data Fig. 9b,c). Furthermore, we found that vacuum drying of the commercial liquid form of the NanoLuc substrate, furimazine, and lyophilization of the substrate dilution buffer did not affect the signals of the assay (Extended Data Fig. 9d).

As plate readers might be difficult to access at point-of-care locations or in the field, we tested a battery-supported portable luminometer (32526-11 Junior LB9509, Berthold Technologies) and found that it detected the same concentration range of CR3022 compared to a Tecan M200 infinite plate reader (Extended Data Fig. 10). The device uses a tube to read samples and, therefore, requires twice or more of the sample volume than in a 384-well plate, which (~2 µl of serum/plasma) is still compatible with the amount of sample generated from a finger prick. Together, our data indicate that both the reagents and instruments required for the spLUC assay are well suited for point-of-care or field applications.

Finally, we sought to determine if the spLUC assay could be compatible with other sample types. First, whole blood samples were collected from six convalescent patients with COVID-19, and plasma samples were prepared in parallel for comparison (Fig. 3b). Remarkably, although the overall signals were lower from whole blood samples, all six samples generated N sensor signals, and four had S sensor signals above control levels with the lyophilized sensors. In comparison, all six patients generated N sensor signals, and five had S sensor signals above cutoff values from the plasma samples. Strong correlations were observed between the whole blood signals and the plasma signals ($R > 0.9$). Fresh and lyophilized sensors showed very little difference in performance.

Next, we tested the potential of using saliva as an input. To determine conditions, we added varying concentrations of the CR3022 antibody into saliva from a healthy individual (Supplementary Fig. 4). We saw a significant reduction in sensitivity for undiluted saliva relative to buffer alone but, remarkably, no loss in sensitivity when the saliva was diluted 1:2 in PBS buffer. We then tested 42 saliva samples at 1:2 dilution with the S sensors. We increased the reaction volume from 20 µl to 100 µl and the luminescence signal integration time from 1,000 ms to 5,000 ms for better sensitivity, as lower antibody concentrations are expected from saliva samples[42]. Of the 42 samples, 33 had signals above the two healthy saliva controls, indicating a 79% assay sensitivity (Fig. 3c). A moderate correlation of saliva signal with corresponding serum signals was observed ($R = 0.66$), consistent with recent reports[43]. These results highlight the potential of using lyophilized sensors/substrates and whole blood or saliva samples for rapid and quantitative point-of-care antibody testing.

Discussion

As SARS-CoV-2 continues to spread, the need will continue to grow for serology assays to determine not only the scope of infection but also vaccine efficacy during clinical trials and after large-scale vaccine deployment. We present here spLUC, a simple, sensitive, specific, fast, low-input sample volume and quantitative solution-phase serological assay to detect antibodies against S and N proteins. We were able to test 159 patient samples across three different cohorts with varying clinical and demographic features. Our results enabled association analysis between these features and antibody titers, demonstrating the promise of this assay to generate large datasets to better understand factors that modulate the humoral response after SARS-CoV-2 infection.

The quantitative and solution-based nature of the spLUC assay allows convenient assay variations. We presented a competitive spLUC assay using epitope-masked S sensors and used it to study the prevalence of an unconventional neutralization epitope in the S-RBD domain. This competitive spLUC assay has the potential to serve as a surrogate virus neutralization assay and to unveil details of the interaction of patient antibodies to viral antigens.

Robust ELISA-based assays, such as the one developed by Krammer and colleagues, have enabled tremendous progress of COVID-19 serological studies[14,24], but these assays are still laborious with multiple wash steps, which limits their broad application for population-scale sero-surveillance, point-of-care diagnostics and deployment in countries or remote areas that have limited access to analytical equipment and reagents. The spLUC assays have important features amenable to these applications. We have shown that our reagents are not only compatible with lyophilization for easy transport and storage but also can readily detect antibodies directly

from whole blood samples and saliva samples. With simple pipettes and a battery-supported portable luminometer, the spLUC assay could be readily established at care centers or in the field worldwide, regardless of infrastructure. To this end, we showed that a commercially available portable luminometer is compatible with this assay, and we are currently collaborating with bioengineers to further develop luminometers that can be manufactured at lower cost but provide equal or better detection sensitivity. We have also shown that the assay is amenable to automation with standard liquid dispenser instruments, which allows for an opportunity to set up automated stations for self-testing at point-of-care locations.

Another important strength of our approach is the modularity. We expect that our strategy can be readily adapted to develop rapid serological tests for immunity against any infectious or autoimmune disease that elicits an antibody response for which the protein antigen is known. Our work identified important protein engineering details in constructing sensitive biosensors against anti-coronavirus antibodies, such as using the RBD domain of the S protein, removing the dimerization domain from the N protein and fusing split enzymes to the C terminus of the N protein. These sensor designs are instructive for a rapid response if we have to face a future pandemic caused by a new strain of coronavirus. Moreover, the spLUC constructs are also nimble for engineering variant RBD domains to assess antibody response to new viral variants that are emerging. These should be useful for determining vaccine effectiveness in communities having multiple viral strains. Future development of our spLUC assay includes exploring orthogonal split enzyme systems to allow multiplexing of assays. For instance, split ß-lactamase, used by Huang and colleagues for detecting herpes simplex virus antibodies[44], can provide an orthogonal readout to luminescence. We envision that such multiplexed assays could be used to develop broad-spectrum serological assays to simultaneously detect immunity against multiple infectious diseases.

In summary, we took a structure-based protein engineering approach to design novel split enzyme-fused sensors. These biosensors enable spLUC, a next-generation SARS-CoV-2 antibody test suited for population-scale sero-surveillance, epitope mapping of patient antibody responses and testing in resource-limited areas. Future efforts will focus on continued evaluation of alternative sample sources, collaboration with industry and clinical labs for broad deployment of the assay and development of similar split enzyme-based serological approaches for a range of infectious diseases.

Online content

Any methods, additional references, Nature Research reporting summaries, source data, extended data, supplementary information, acknowledgements, peer review information; details of author contributions and competing interests; and statements of data and code availability are available at https://doi.org/10.1038/s41587-021-00878-8.

Received: 10 August 2020; Accepted: 2 March 2021;
Published online: 25 March 2021

References

1. Krammer, F. & Simon, V. Serology assays to manage COVID-19. *Science* **368**, 1060–1061 (2020).
2. Lynch, K. L. et al. Magnitude and kinetics of anti-SARS-CoV-2 antibody responses and their relationship to disease severity. *Clin. Infect. Dis.* **72**, 301–308 (2020).
3. Okba, N. M. A. et al. Severe acute respiratory syndrome coronavirus 2-specific antibody responses in coronavirus disease patients. *Emerg. Infect. Dis.* **26**, 1478–1488 (2020).
4. Seow, J. et al. Longitudinal observation and decline of neutralizing antibody responses in the three months following SARS-CoV-2 infection in humans. *Nat. Microbiol.* **5**, 598–1607 (2020).
5. Smith, T. R. F. et al. Immunogenicity of a DNA vaccine candidate for COVID-19. *Nat. Commun.* **11**, 2601 (2020).
6. Yu, J. et al. DNA vaccine protection against SARS-CoV-2 in rhesus macaques. *Science* **369**, 806–811 (2020).
7. van Doremalen, N. et al. ChAdOx1 nCoV-19 vaccine prevents SARS-CoV-2 pneumonia in rhesus macaques. *Nature* **586**, 578–582 (2020).
8. Long, Q.-X. et al. Antibody responses to SARS-CoV-2 in patients with COVID-19. *Nat. Med.* **26**, 845–848 (2020).
9. To, K. K.-W. et al. Temporal profiles of viral load in posterior oropharyngeal saliva samples and serum antibody responses during infection by SARS-CoV-2: an observational cohort study. *Lancet Infect. Dis.* **20**, 565–574 (2020).
10. Zhao, J. et al. Antibody responses to SARS-CoV-2 in patients of novel coronavirus disease 2019. *Clin. Infect. Dis.* **71**, 2027–2034 (2020).
11. Casadevall, A. & Pirofski, L.-a The convalescent sera option for containing COVID-19. *J. Clin. Invest.* **130**, 1545–1548 (2020).
12. Robbiani, D. F. et al. Convergent antibody responses to SARS-CoV-2 in convalescent individuals. *Nature* **584**, 437–442 (2020).
13. Rogers, T. F. et al. Isolation of potent SARS-CoV-2 neutralizing antibodies and protection from disease in a small animal model. *Science* **369**, 956–963 (2020).
14. Amanat, F. et al. A serological assay to detect SARS-CoV-2 seroconversion in humans. *Nat. Med.* **26**, 1033–1036 (2020).
15. Tan, W. et al. Viral kinetics and antibody responses in patients with COVID-19. Preprint at medRxiv https://doi.org/10.1101/2020.03.24.20042382 (2020).
16. Xiang, J. et al. Evaluation of enzyme-linked immunoassay and colloidal gold-immunochromatographic assay kit for detection of novel coronavirus (SARS-Cov-2) causing an outbreak of pneumonia (COVID-19). Preprint at *medRxiv* https://doi.org/10.1101/2020.02.27.20028787 (2020).
17. Li, Z. et al. Development and clinical application of a rapid IgM-IgG combined antibody test for SARS-CoV-2 infection diagnosis. *J. Med. Virol.* **92**, 1518–1524 (2020).
18. Lassaunière, R. et al. Evaluation of nine commercial SARS-CoV-2 immunoassays. Preprint at *medRxiv* https://doi.org/10.1101/2020.04.09.20056325 (2020).
19. Whitman, J. D. et al. Evaluation of SARS-CoV-2 serology assays reveals a range of test performance. *Nat. Biotechnol.* **38**, 1174–1183 (2020).
20. Dixon, A. S. et al. NanoLuc complementation reporter optimized for accurate measurement of protein interactions in cells. *ACS Chem. Biol.* **11**, 400–408 (2016).
21. Letko, M., Marzi, A. & Munster, V. Functional assessment of cell entry and receptor usage for SARS-CoV-2 and other lineage B betacoronaviruses. *Nat. Microbiol.* **5**, 562–569 (2020).
22. Kang, S. et al. Crystal structure of SARS-CoV-2 nucleocapsid protein RNA binding domain reveals potential unique drug targeting sites. *Acta Pharm. Sin. B* **10**, 1228–1238 (2020).
23. Qu, J. et al. Profile of IgG and IgM antibodies against severe acute respiratory syndrome coronavirus 2 (SARS-CoV-2). *Clin. Infect. Dis.* **71**, 2255–2258 (2020).
24. Stadlbauer, D. et al. SARS-CoV-2 seroconversion in humans: a detailed protocol for a serological assay, antigen production, and test setup. *Curr. Protoc. Microbiol* **57**, e100 (2020).
25. Zhao, J. et al. Comparison of immunoglobulin G responses to the spike and nucleocapsid proteins of severe acute respiratory syndrome (SARS) coronavirus in patients with SARS. *Clin. Vaccine Immunol.* **14**, 839–846 (2007).
26. Byrnes, J. R. et al. Competitive SARS-CoV-2 serology reveals most antibodies targeting the spike receptor-binding domain compete for ACE2 binding. *mSphere* **5**, e00802-20 (2020).
27. Rosado, J. et al. Multiplex assays for the identification of serological signatures of SARS-CoV-2 infection: an antibody-based diagnostic and machine learning study. *Lancet Microbe* **2**, e60–e69 (2021).
28. Barnes, C. O. et al. Structures of human antibodies bound to SARS-CoV-2 spike reveal common epitopes and recurrent features of antibodies. *Cell* **182**, 828–842 (2020).
29. Yuan, M. et al. A highly conserved cryptic epitope in the receptor binding domains of SARS-CoV-2 and SARS-CoV. *Science* **368**, 630–633 (2020).
30. Glasgow, A. et al. Engineered ACE2 receptor traps potently neutralize SARS-CoV-2. *Proc. Natl Acad. Sci. USA* **117**, 28046–28055 (2020).
31. Poulsen, T. R., Meijer, P.-J., Jensen, A., Nielsen, L. S. & Andersen, P. S. Kinetic, affinity, and diversity limits of human polyclonal antibody responses against tetanus toxoid. *J. Immunol.* **179**, 3841–3850 (2007).
32. Reddy, S. B. et al. Differences in affinity of monoclonal and naturally acquired polyclonal antibodies against *Plasmodium falciparum* merozoite antigens. *BMC Microbiol.* **15**, 1–11 (2015).
33. Zamecnik, C. R. et al. ReScan, a multiplex diagnostic pipeline, pans human sera for SARS-CoV-2 antigens. *Cell Rep. Med.* **1**, 100123 (2020).
34. Burbelo, P. D. et al. Sensitivity in detection of antibodies to nucleocapsid and spike proteins of severe acute respiratory syndrome coronavirus 2 in patients with Coronavirus Disease 2019. *J. Infect. Dis.* **222**, 206–213 (2020).
35. Tan, C. W. et al. A SARS-CoV-2 surrogate virus neutralization test based on antibody-mediated blockage of ACE2-spike protein–protein interaction. *Nat. Biotechnol.* **38**, 1073–1078 (2020).
36. Mäkelä, O., Ruoslahti, E. & Seppälä, I. J. Affinity of IgM and IgG antibodies. *Immunochemistry* **7**, 917–932 (1970).

37. Wajnberg, A. et al. Robust neutralizing antibodies to SARS-CoV-2 infection persist for months. *Science* **370**, 1227–1230 (2020).
38. Cervia, C. et al. Systemic and mucosal antibody responses specific to SARS-CoV-2 during mild versus severe COVID-19. *J. Allergy Clin. Immunol.* **147**, 545–557 (2020).
39. Klein, S. L. et al. Sex, age, and hospitalization drive antibody responses in a COVID-19 convalescent plasma donor population. *J. Clin. Invest.* **130**, 6141–6150 (2020).
40. Hornsby, M. et al. A high through-put platform for recombinant antibodies to folded proteins. *Mol. Cell Proteom.* **14**, 2833–2847 (2015).
41. Denkinger, C. M. et al. Guidance for the evaluation of tuberculosis diagnostics that meet the World Health Organization (WHO) target product profiles: an introduction to who process and study design principles. *J. Infect. Dis.* **220**, S91–S98 (2019).
42. Pisanic, N. et al. COVID-19 serology at population scale: SARS-CoV-2-specific antibody responses in saliva. *J. Clin. Microbiol.* **1**, e02204-20 (2021).
43. Faustini, S. E. et al. Detection of antibodies to the SARS-CoV-2 spike glycoprotein in both serum and saliva enhances detection of infection. Preprint at *medRxiv* https://doi.org/10.1101/2020.06.16.20133025 (2020).
44. Fry, S. R. et al. Detection of HSV type-1 and type-2 IgG using an in vitro PCA based homogeneous immunoassay. *Biochem. Biophys. Res. Commun.* **372**, 542–546 (2008).

Publisher's note Springer Nature remains neutral with regard to jurisdictional claims in published maps and institutional affiliations.

© The Author(s), under exclusive licence to Springer Nature America, Inc. 2021

Methods

Plasmid construction. Plasmids were constructed by standard molecular biology methods. The DNA fragments of Spike-RBD, N protein, ACE2 and LgBiT were synthesized by IDT Technologies. The SmBiT tag was generated by overlap extension PCR. The Spike-RBD-5/15/25aa-LgBiT-12xHisTag, Spike-RBD-15/25aa-SmBiT-12xHisTag, N protein(44–180)-10aa-LgBiT-12xHisTag, N protein(44–180)-10aa-SmBiT-12xHisTag, LgBiT-10aa-N protein(44–257)-12xHisTag and SmBiT-10aa-N protein(44–257)-12xHisTag were generated by subcloning into a pFUSE-12xHisTag vector (adapted from the pFUSE-hIgG1-Fc vector from InvivoGen). The ACE2-Fc fusion plasmids were generated by subcloning the gene fragments of ACE2 and mutant into the pFUSE-hIgG1-Fc vector. The C004, C105 and C135 IgG LC and HC plasmids were a generous gift from the Nussenzweig lab (Rockefeller University). The CR3022 IgG plasmids were a generous gift from the Kim lab (Stanford University) and the Wilson lab (Scripps Research Institute). The C135 Fab was cloned by removing the Fc domain from the HC plasmid. SnapGene and ApE were used for cloning design and sequence verification.

Expression and protein purification. All proteins were expressed and purified from Expi293 BirA cells according to established protocols from the manufacturer (Thermo Fisher Scientific). Briefly, 30 µg of pFUSE (InvivoGen) vector encoding the protein of interest was transiently transfected into 75 million Expi293 BirA cells using the ExpiFectamine kit (Thermo Fisher Scientific). For the IgG and Fab proteins, 15 µg of each chain was transfected. Enhancer was added 20 h after transfection. Cells were incubated for a total of 3 d at 37 °C in an 8% CO_2 environment before the supernatants were harvested by centrifugation. Fc-fusion proteins were purified by protein A affinity chromatography, and His-tagged proteins were purified by Ni-NTA affinity chromatography. Purity and integrity were assessed by SDS/PAGE. Purified protein was buffer exchanged into PBS and stored at −80 °C in aliquots. Concentration was verified by absorbance on a NanoDrop with NanoDrop 2000c software.

Solution serology protocol for in vitro, serum, blood, and saliva samples. LgBiT and SmBiT sensors for either the Spike or N protein were prepared at a final concentration of each sensor at 2 nM in PBS + 0.05% Tween-20 + 0.2% BSA (PBSTB). For in vitro IgGs or ACE2-Fc, the samples were prepared at 1:10 dilutions in PBSTB unless otherwise specified. Serum and blood samples were diluted to 1:12.5 for both the S and N sensor samples in PBSTB unless otherwise specified. Healthy individual saliva was spiked in with CR3022 and used undiluted or diluted 1:2 in PBSTB. Then, 10 µl of the 2 nM sensor mix and 10 µl of the sample were combined in a 384 Lumitrac white plate (Greiner), skipping every other well and row to avoid potential bleedover in signal. The plate was mixed on a plate shaker for 20 min. NanoLuc substrate was diluted according to protocol 1:50 in NanoLuc dilution buffer (Promega), and 15 µl was added to each well, followed by a 10-min incubation period for the signal to stabilize. Luminescence was measured on a Tecan M200 infinite plate reader with an integration time of 1,000 ms. Tecan i-control plate reader software was used for data acquisition.

Competition serology protocol for in vitro and serum samples. The competition serology assay was performed similarly to the solution serology assay except that the S sensors were individually pre-incubated at 4 nM with 4 µM of C004 Fab, C105 Fab or C135 Fab for the in vitro competition assay and C135 Fab only for the serum competition assay. The two sensors + Fab were combined 1:1 to make a 2 nM mix, and 10 µl of this mix was added to the assay as described above.

Epitope binning experiment. Biolayer interferometry data were measured using an Octet RED384 (ForteBio). Biotinylated Spike RBD protein was immobilized on the streptavidin biosensor (ForteBio). After blocking with biotin, the sensor was loaded with one IgG followed by another IgG or ACE2-Fc to determine epitope binning. PBS with 0.05% Tween-20 and 0.2% BSA was used for all diluents and buffers. ForteBio Octet Data Acquisition software was used for acquiring data, and ForteBio Octet Data Analysis software was used for analyzing data.

Spike protein ELISA assay. The Spike ELISA assay was performed as previously described. Briefly, 384 MaxiSorp plates were coated with 100 µl of 0.5 µg ml^{-1} NeutrAvidin for 1 h. The plate was washed three times with PBS + 0.05% Tween-20 (PBST) followed by incubation with 20 nM S-RBD for 30 min. After three washes, the plate was blocked with 3% non-fat milk in PBS for 1 h. The plate was washed three times before the addition of 1:50 dilutions of serum in 1% non-fat milk for 1 h. After three washes, secondary anti-human Fab (Jackson ImmunoResearch Laboratories, 109-036-097 (1:5,000)), anti-human IgM (Sigma-Aldrich, A6907 (1:3,000)) or anti-human IgG (Sigma-Aldrich, A0170 (1:3,000)) antibody was added and incubated for 30 min before the addition of TMB for 3 min. The reaction was quenched with 1 M phosphoric acid, and absorbance was read on a Tecan M200 infinite plate reader at 450 nm.

Inter-day and intra-day assay with liquid dispensers. Plasma was diluted 12.5-fold into a 96-well plate, and, subsequently, 10 µl was dispensed into an individual flat-bottom white plate (Greiner Lumitrac 200, 384-well plates) using a Biomek FX^P Automated Workstation (Beckmann Coulter). Next, 10 µl of 1 nM biosensors was dispensed using Thermo Multidrop Combi Reagent Dispenser (Thermo Fisher Scientific) to assay plates and incubated at room temperature for 20 min. Then, 15 µl of substrate was added using the same reagent dispenser and incubated at room temperature for 10 min. Luminescence was read on a Tecan M200 infinite plate reader with an integration time of 1,000 ms.

Simulated automation of the spLUC assay on a robotic platform. To facilitate high-throughput screening of serum, a semi-automated approach was developed and simulated using the UCSF Antibiome Center robotics platform[40]. Serum in 96-well plates is first diluted 12.5-fold, and 10 µl is dispensed into four individual flat-bottom white plates (Greiner Lumitrac 200, 384-well plates) using a Biomek FX^P Automated Workstation (Beckmann Coulter). Serum-containing assay plates are then transferred to a robotics protocol with dispensing of biosensor and substrate followed by luminescence reading. Although one iteration of 96 samples takes 40 min, each additional iteration takes an additional 3.5 min, limited by luminescence reading (1 s per well plus plate transfer). As such, it is estimated that 40 plates (3,840 assays) could be run in 3 h. The robotics run was developed and simulated using Thermo Momentum software (v5.0.6).

Lyophilization of sensors and dilution buffer. The S and N protein sensors were flash frozen in liquid nitrogen at concentrations between 10 µM and 60 µM in 10 µl. The dilution buffer was frozen in liquid nitrogen in 5-ml aliquots. A small hole was poked into the caps of the samples and left on a BenchTop K (VirTis) lyophilizer overnight. The next day, the sensors were reconstituted in 10 µl of double-distilled water (ddH_2O), and concentration was verified by NanoDrop. The dilution buffer was similarly reconstituted in 5 ml of ddH_2O.

Vacuum-dried centrifugation of substrate sample. Next, 20 µl of substrate was aliquoted in a dark Eppendorf tube and subjected to vacuum centrifugation overnight on a Genevac instrument. The substrate was stored in the dark for 2 d at room temperature before reconstitution in 20 µl of 100% methanol. The substrate was diluted 1:50 as normal in dilution buffer for the assay.

Serum, plasma, whole blood and saliva samples. The initial small patient cohort was a generous gift from the Wilson lab (UCSF) and heat inactivated at 56 °C for 1 h before storage at −80 °C. The first (outpatient) sample serum set (Cohort 1) was a generous gift from the Wilson lab (UCSF) and the Nussenzweig lab (Rockefeller University). These samples were heat inactivated at 56 °C for 1 h and stored at 4 °C in a 1:1 dilution in 40% glycerol, 40 mM HEPES (pH 7.3) and 0.04% NaN_3 in PBS. The second (inpatient) sample serum set (Cohort 2) was a generous gift from the Wang lab (Stanford University) and was stored at −80 °C as pure serum samples. The third plasma cohort (Cohort 3) and blood samples were generous gifts from the Greenhouse lab (UCSF) and the Henrich Lab (UCSF) as part of the LIINC study. The plasma samples were stored at 4 °C in a 1:1 dilution in 40% glycerol, 40 mM HEPES (pH 7.3) and 0.04% NaN_3 in PBS. The whole blood was stored undiluted at 4 °C. Healthy blood samples were purchased from Vitalant and stored undiluted at 4 °C. The saliva samples were obtained as unstimulated, unexpectorated saliva and were stored at −80 °C. Before being assayed, the samples were thawed and centrifuged at 9,000*g* to remove any insoluble or coagulated matter. Control saliva from November 2019 was purchased from Lee Biosolutions, stored at −20 °C and processed similarly.

Data and statistical analysis. All graphing and statistical analysis were performed in GraphPad Prism or Microsoft Excel. The unpaired multiple *t*-test was performed in Prism to compare conditions in each patient for the competition spLUC assay. The non-parametric Spearman correlation analysis was used in Prism to determine the correlation *R* value between datasets. When two groups were compared, an unpaired Mann–Whitney test was performed to determine the difference between datasets. For comparison of three or more groups, a Kruskal–Wallis test with Dunn's multiple comparison post hoc testing was used. A two-tailed *P* value was used to determine statistical significance for all analysis. $P < 0.05$ was considered statistically significant.

Ethics declaration. All patient samples were obtained under protocols approved by the institutional review boards (IRBs) and in accordance with the Declaration of Helsinki. Samples were de-identified before delivery to the lab where all assays described here were performed. Cohort 1 samples were a kind gift from M. Nussenzweig, M. Caskey and C. Gaebler of Rockefeller University, collected under Rockefeller IRB protocol DRO-1006. Cohort 2 samples from Kaiser Permanente were collected under Stanford University IRB protocol 55718. Cohort 3 samples were collected under UCSF IRB protocol 20-30479. Influenza virus vaccination samples were from a US cohort enrolled at the Rockefeller University Hospital in New York City in 2012–2013 under a protocol approved by the IRB of Rockefeller University (protocol TWA-0804). Samples from people with seasonal coronavirus infections were collected at the University of Chicago. Samples were de-identified serums of healthcare workers who had respiratory illnesses, were swabbed and tested positive for common cold coronavirus infections in 2019 (University of Chicago protocol 09-043-A).

Reporting Summary. Further information on research design is available in the Nature Research Reporting Summary linked to this article.

Data availability

The datasets generated and/or analyzed during the current study are available from the corresponding author (J.A.W.) upon reasonable request. Datasets 6XCN, 6W41, 1N8Z, 5IBO and 5D6D used for modeling were downloaded from the Protein Data Bank. Source data are provided with this paper.

Code availability

R scripts used for ordinary differential equation modeling are available for download at https://github.com/alexmartinko/Serological_ODE_Model.

Acknowledgements

We acknowledge the members of the Wells Lab, especially those involved in our COVID-19 research program. We also acknowledge M. Nussenzweig, M. Caskey and C. Gaebler (Rockefeller University) as well as C. Zamecnik, M. Wilson and J. DeRisi (UCSF) for providing the first cohort of convalescent sera. We thank M. Nussenzweig and D. Robbiani (Rockefeller University) for providing plasmids for C004, C105 and C135 IgGs. We thank P. Kim (Stanford University) and I. Wilson (Scripps Research) for providing the plasmid for CR3022. We additionally thank P. Wilson (University of Chicago) for the seasonal coronavirus control samples. We thank M. Lin, X. Shu and C. Chiu for helpful discussions. We thank all the patients for their participation in this study. J.A.W. is grateful for funding from the Harry and Dianna Hind Endowed Professorship in Pharmaceutical Sciences and the Chan Zuckerberg Biohub that helped support this work. The National Science Foundation Graduate Research Fellowship Program supported S.K.E. (1650113) and I.L. (1650113). Postdoctoral fellowship support included a Merck Fellowship of the Damon Runyon Cancer Research Foundation (DRG-2297-17 to X.X.Z.), a National Institutes of Health K99/R00 award (1K99EB030587-01 to X.X.Z.), a National Institutes of Health National Cancer Institute F32 (5F32CA239417 to J.R.B.), a Merck Postdoctoral Research Fellowship from the Helen Hay Whitney Foundation (S.A.L.) and a National Institutes of Health K99/R00 (1K99GM135529 to A.A.G.). The LIINC cohort study was funded by NIH/NIAID 3R01AI141003-03S1 (T.J.H.). T.T.W. was supported, in part, by Fast Grants, the CEND COVID Catalyst Fund, the NIH/NIAID (U19AI111825 and R01AI139119) and the Rockefeller University Center for Clinical and Translational Science Grant no. UL1 TR001866. We would also like to acknowledge funding from the Chan Zuckerberg Biohub, Rapid Response.

Author contributions

S.K.E., X.X.Z. and J.A.W. conceived the study, designed the research and wrote the manuscript. S.K.E. and X.X.Z. designed the experiments and analyzed the data. S.K.E. performed the experiments, unless otherwise stated. X.X.Z. performed structure modeling and analysis for sensor design. J.R.B. performed the anti-Fab ELISA experiments, provided advice for the whole blood work and co-wrote the manuscript. K.K.L. designed the robotic workflow and co-wrote the manuscript. A.J.M. performed the in silico differential equation modeling and analyzed the data. I.L., K.P. and S.A.L. helped with expression and purification and performed the ACE2 epitope binning experiment. J.E.G. and A.A.G. designed, expressed and purified the higher-affinity ACE2 mutant. T.T.W. provided patient sera and control sera samples. T.J.H., M.J.P., B.G., N.S.I., L.T. and K.T. provided patient samples and oversaw LIINC sample collections, sample processing, sample maintenance and cohort design. B.G. and C.M.T. provided helpful discussions. X.X.Z. and J.A.W. supervised the research. All authors edited and approved the final manuscript version.

Competing interests

S.K.E., X.X.Z. and J.A.W. have filed a provisional patent on the solution-based spLUC assay. J.E.G., A.A.G., I.L., X.X.Z. and J.A.W. have filed a provisional patent on the ACE2 variants.

Additional information

Extended data is available for this paper at https://doi.org/10.1038/s41587-021-00878-8.

Supplementary information The online version contains supplementary material available at https://doi.org/10.1038/s41587-021-00878-8.

Correspondence and requests for materials should be addressed to J.A.W.

Peer review information *Nature Biotechnology* thanks Harry Ostrer, Kevin Nichols and the other, anonymous, reviewer(s) for their contribution to the peer review of this work.

Reprints and permissions information is available at www.nature.com/reprints.

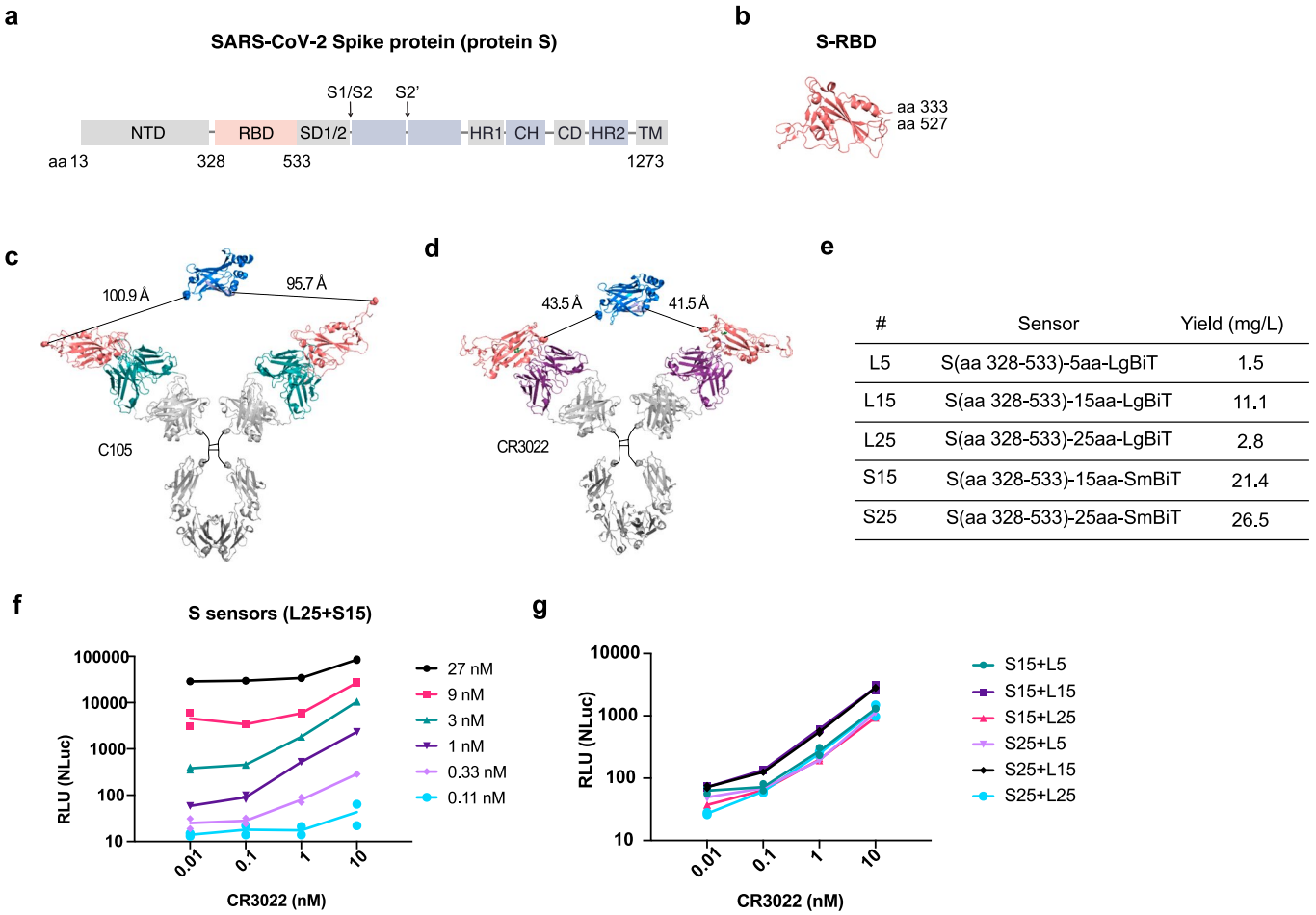

#	Sensor	Yield (mg/L)
L5	S(aa 328-533)-5aa-LgBiT	1.5
L15	S(aa 328-533)-15aa-LgBiT	11.1
L25	S(aa 328-533)-25aa-LgBiT	2.8
S15	S(aa 328-533)-15aa-SmBiT	21.4
S25	S(aa 328-533)-25aa-SmBiT	26.5

Extended Data Fig. 1 | Design and characterization of S sensors. a, Annotated depiction of the SARS-CoV-2 Spike protein. The S sensors were developed using only the S-RBD domain (aa 328–533, PDB: 6W41) shown in pink. **b**, Structure of the S-RBD domain shows the N and C termini locate in close proximity. **c, d**, Modeling of c, ACE2-competitive antibody C105 (PDB: 6XCN) binding to S-RBD-SmBiT/LgBiT sensors, and d, CR3022 (PDB: 6W41) binding to S-RBD-SmBiT/LgBiT sensors. Modeling and distance measurements were performed with PDB 6XCN, 6W41, 1N8Z, 5IBO and 5D6D in PyMOL. **e**, Yield of the 5 Spike-NanoBiT sensor fusions. The Spike LgBiT sensors were made with 5aa, 15aa, and 25aa Glycine-Serine (GS) linkers (L5, L15 and L25). The Spike SmBiT sensors were made with 15aa, and 25aa GS linkers (S15 and S25). Because the N and C termini of the S-RBD domain locate in close proximity, only fusions to the C termini of S-RBD were constructed. **f**, The S sensors are most sensitive at 1 nM for detecting CR3022 in solution compared to higher or lower sensor concentrations. Two technical replicates are plotted from n=1 individual experiment. Lines connecting the means of the samples are plotted. **g**, S sensors with varied linker lengths resulted in very similar signal strength in detecting CR3022. Two technical replicates are plotted from n=1 individual experiment. Lines connecting the means of the samples are plotted.

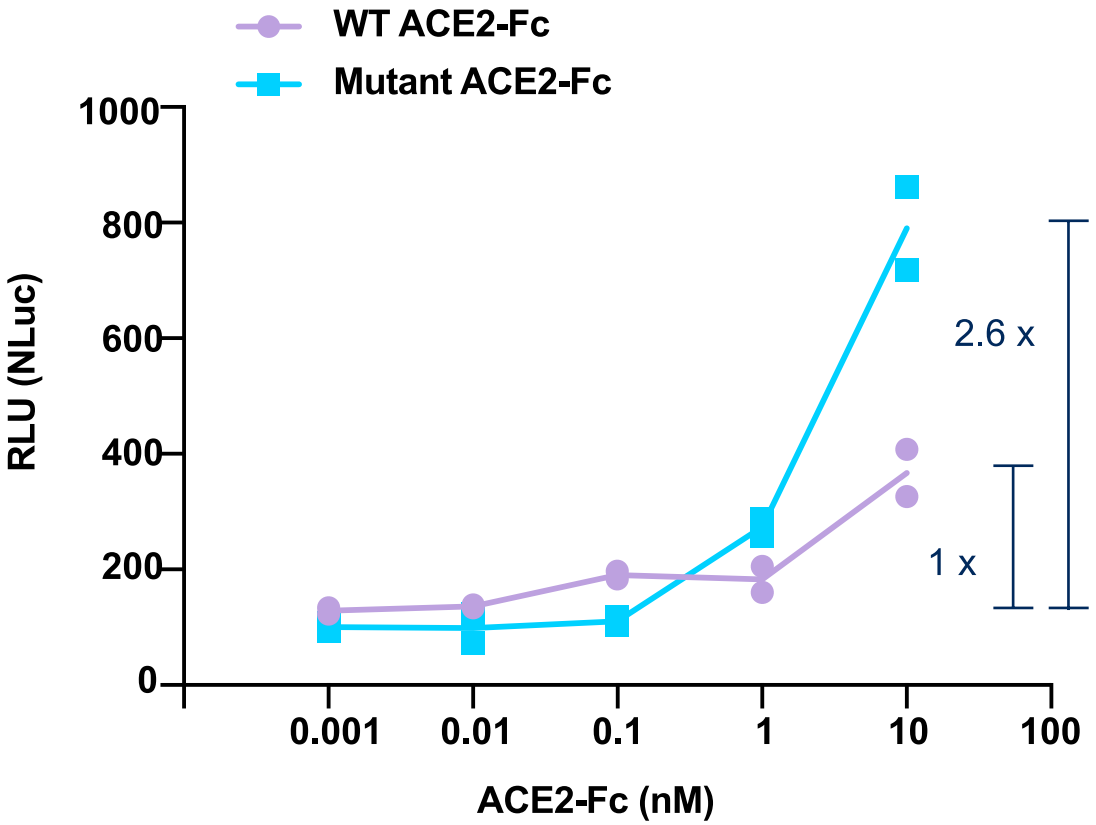

Extended Data Fig. 2 | The biosensors are more sensitive to high-affinity binders. The ACE2-Fc variant which binds 10-fold tighter to S-RBD generated ~3-fold higher signal at 10 nM protein concentration comparing to WT ACE2-Fc. Two technical replicates are plotted from n=1 individual experiment. Lines connecting the means of the samples are plotted.

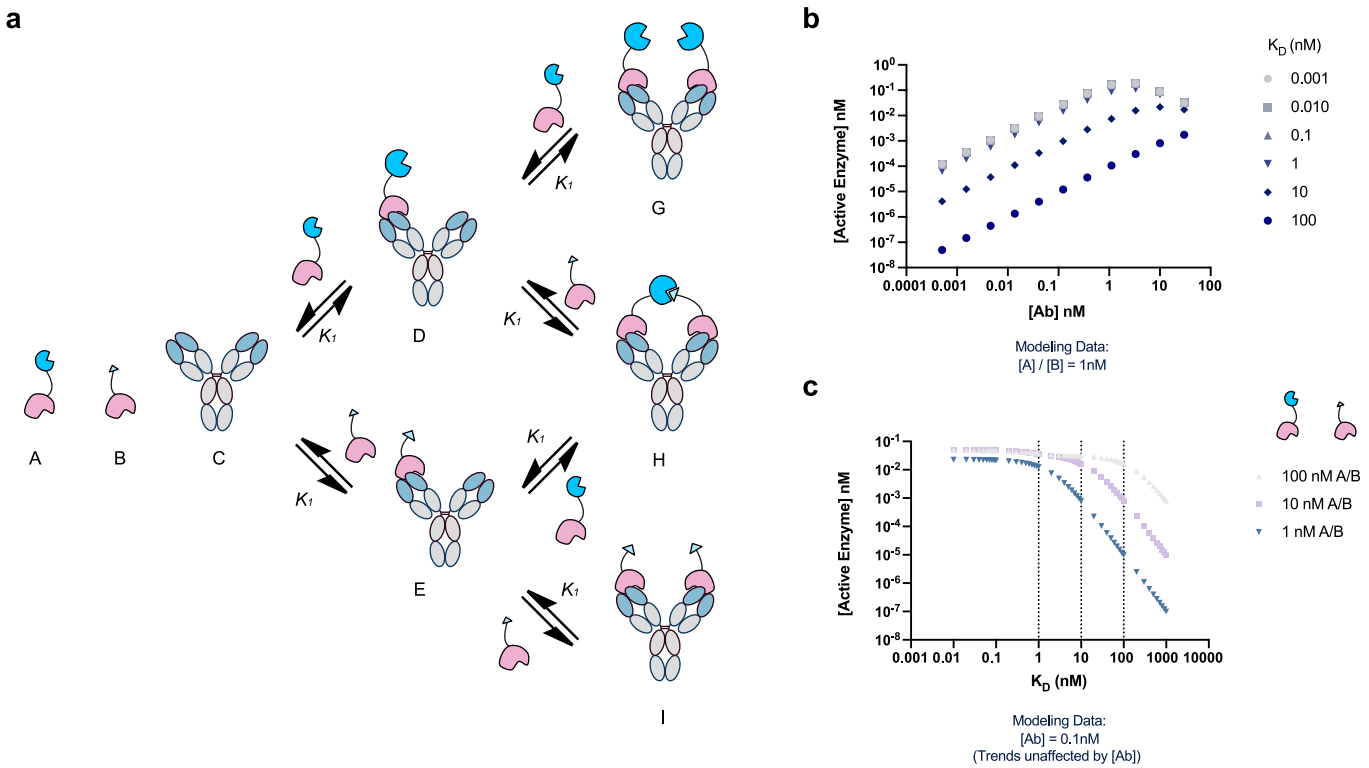

Extended Data Fig. 3 | ODE models predict a linear, dose-dependent response and K_D dependence of the luminescence signal. a, Antibody (C) and sensor components (A and B) are in thermodynamic equilibrium with enzymatically inactive (D, E, G, and I) and active (H) sensor bound species. **b**, At 1 nM starting concentration of sensor ([A] and [B]), spLUC assays are predicted to generate signals linearly correlated to a broad range of antibody concentrations ([Ab]). Signal is predicted to be insensitive to antibody concentrations for antibodies with high affinity for the sensor ($\leq$ 1nM), but weaker affinity antibodies (K_D > 1 nM) will result in significantly lower levels of reconstituted enzyme. **c**, At K_D values equivalent or higher than the sensor concentrations, the spLUC signals are predicted to drop significantly.

a

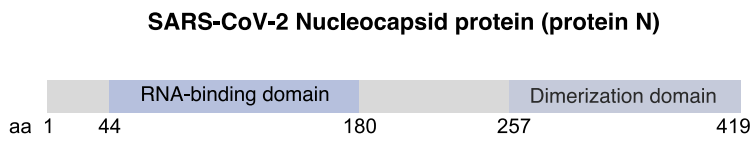

b

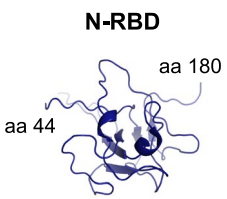

c

#	Sensor	Yield (mg/L)
LC	N(aa 44-180)-10aa-LgBiT	6.4
SC	N(aa 44-180)-10aa-SmBiT	14.2
LC2	N(aa 44-257)-10aa-LgBiT	11.2
SC2	N(aa 44-257)-10aa-SmBiT	1.8
LN	LgBiT-10aa-N(aa 44-257)	1.6
SN	SmBiT-10aa-N(aa 44-257)	6.8

d

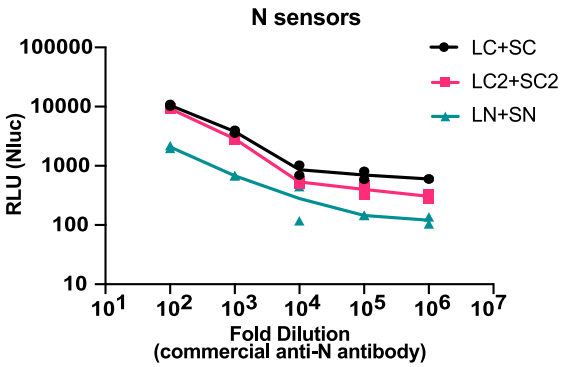

e

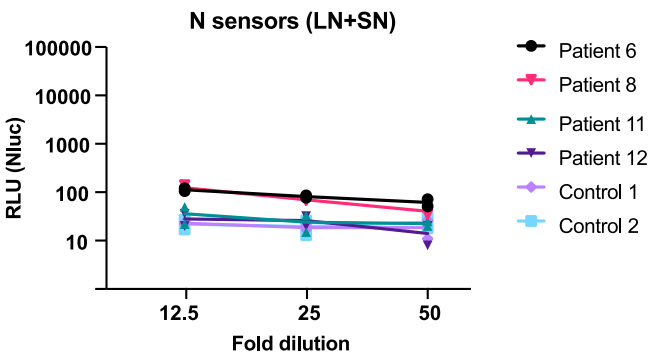

Extended Data Fig. 4 | Design and characterization of N sensors. a, Annotated depiction of the SARS-CoV-2 Nucleocapsid protein (protein N). All N protein fusions designed included the RNA binding domain (aa 44–180, N-RBD) and excluded the dimerization domain (aa 257–419). **b**, Structure of the N-RBD domain shows the N and C termini locate far from each other and fusion of the split enzyme fragments to N or C termini may result in different detection sensitivity (PDB: 6YI3). **c**, Yield of the six N protein-NanoBiT sensor fusions. **d**, The N-terminal N sensor pair (LN + SN, 44–257) was less sensitive than the LC + SC (44–180) and LC2 + SC2 (44–257) C terminal N sensor pairs when the assay was performed on a rabbit polyclonal anti-N protein antibody (Sino Biological, Cat#: 40588-T62-50). Two technical replicates are plotted from n=1 individual experiment. Lines connecting the means of the samples are plotted. **e**, Additionally, only patient 6 and 8 showed signals above controls in the serological assay performed with LN + SN sensors, while all four patients showed signals with the LC + SC sensors. Two technical replicates are plotted from n = 1 independent experiment. Lines connecting the means of the samples are plotted.

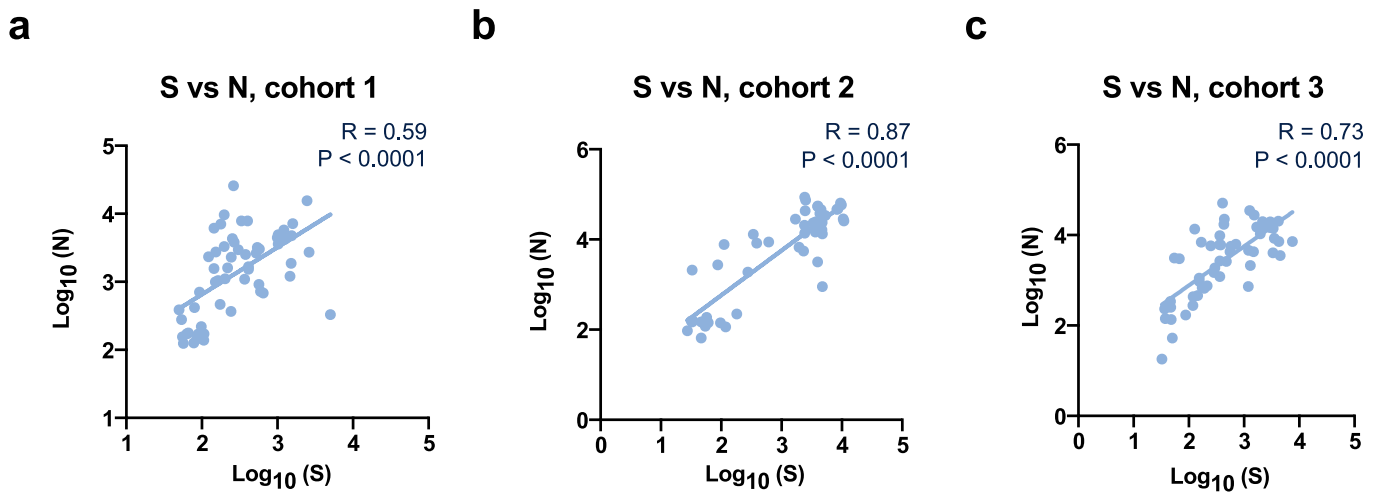

Extended Data Fig. 5 | Individual cohorts show good correlation between S and N sensors. Each cohort shows robust correlation with R = 0.59, 0.87, and 0.73 for **a**, cohort 1 (56 samples), **b**, cohort 2 (47 samples), and **c**, cohort 3 (87 samples), respectively. R values and P values (two-tail) of a non-parametric Spearman correlation analysis are labeled in the graphs. Lines represent linear regression. For all graphs, dots represent the average of two technical replicates from n=1 independent experiment.

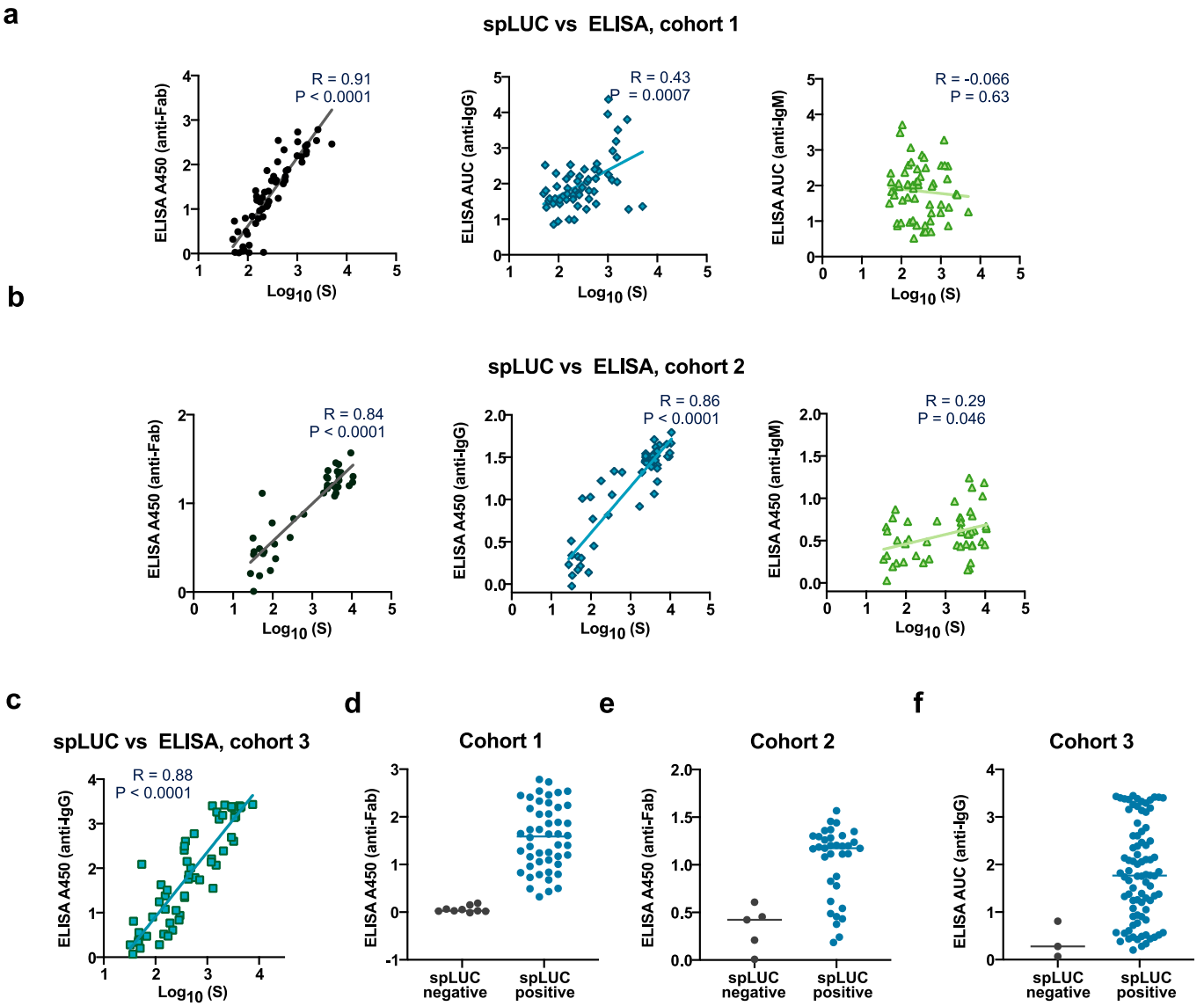

Extended Data Fig. 6 | Comparison of the ELISA and the spLUC results. a, Signals from the S sensor spLUC assay (cohort 1, 57 samples) correlate very well with S-RBD ELISA anti-Fab signals (R = 0.91), moderately well with anti-IgG signals (R = 0.43), and poorly with anti-IgM signals for cohort 1 (R = −0.066). Line represents linear regression. **b**, Signals from the S sensor spLUC assay (cohort 2, 40 samples with anti-Fab detection, 47 samples with anti-IgM/IgG detection) correlate very well with S-RBD ELISA anti-Fab signals (R = 0.84) and with anti-IgG signals (R = 0.86), but poorly with anti-IgM signals for cohort 1 (R = 0.29). Line represents linear regression. **c**, Signals from the S sensor (cohort 3, 87 samples) correlate well with S-RBD ELISA anti-IgG signals (R = 0.88). For a-c, R values and P values (two-tail) of a non-parametric Spearman correlation analysis are labeled in the graphs. Lines represent linear regression. **d, e, f**, The seronegative samples in the anti-S spLUC assay also showed low anti-Fab or anti-IgG signals in ELISA serology tests for **d**, cohort 1 (negative samples (9), positive samples (48)), **e**, cohort 2, (negative samples (5), positive samples (35)), and **f**, cohort 3, (negative samples (3), positive samples (53)). Horizontal lines represent the median value. For all graphs, dots represent the average of two technical replicates from n=1 independent experiment.

a

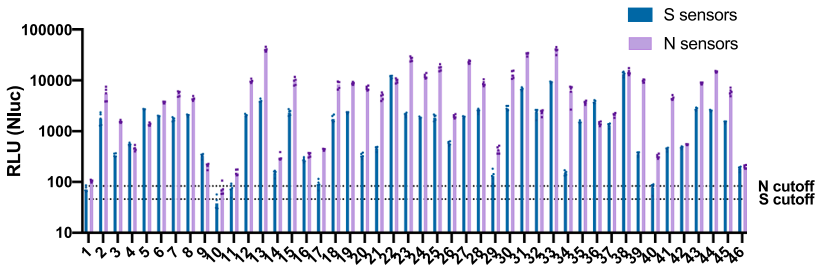

b

Coefficient of variation

	Intra-assay	Intra-day	Inter-day
S sensor	6%	7%	8%
N sensor	6%	9%	9%

Extended Data Fig. 7 | Inter-assay, Inter-day and Intra-day variability of spLUC assay. a, 46 plasma samples were assayed a total of five times in three independent experiments over two days for each sensor. All five replicates are plotted on the graph, with the bar representing the average. The dotted line represents the cutoff values for positive and negative samples for the S and N sensors. **b**, The coefficient of variation was calculated for intra-assay, intra-day, and inter-day variability. Coefficient of variation is calculated as ratio of standard deviation to the average value.

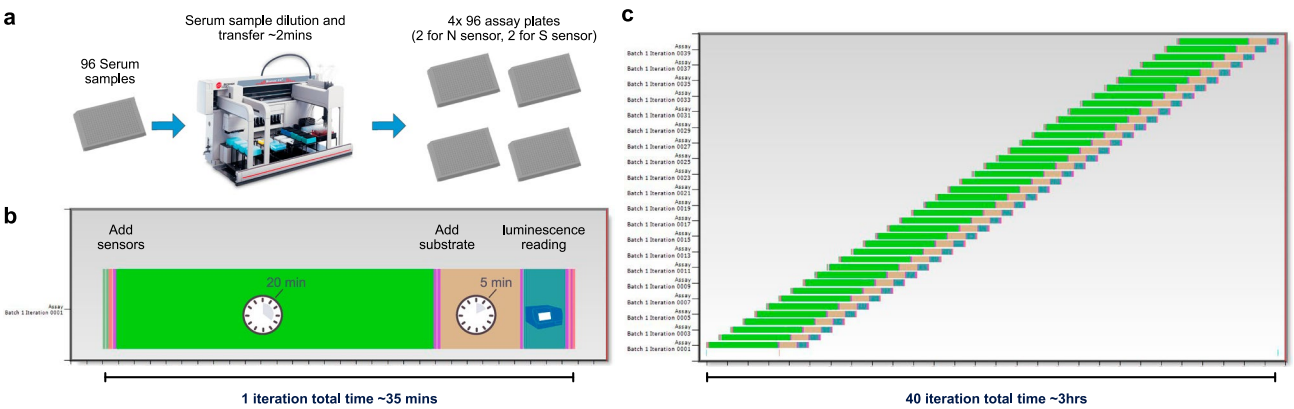

Extended Data Fig. 8 | Simulated robotics-assisted spLUC assay. a, Serum sample transfer to an assay plate using Biomek Fx Automated Workstation in ~2 minutes. **b**, Robotics-assisted dispensing and luminescence reading for one iteration of 96 assays takes ~35 minutes. **c**, Simulated run for 40 iterations (3840 assays) can be completed in 3 hours. Gantt chart generated by simulated run using Thermo Momentum software.

a

Effect of biosensor lyophilization

		% recovery	% signal
S sensor	SmBiT	90	50
	LgBiT	100	
N sensor	SmBiT	70	100
	LgBiT	100	

b

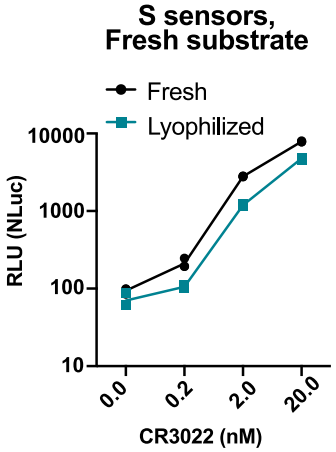

c

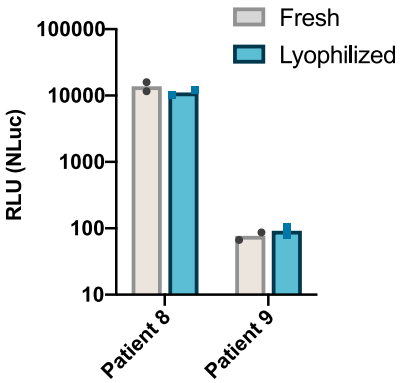

d

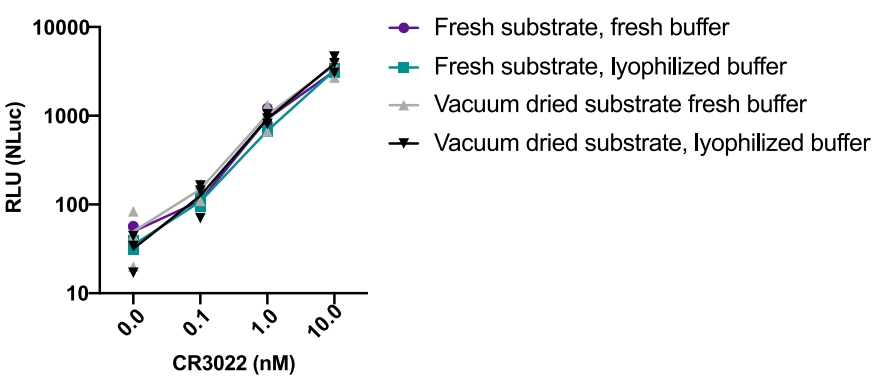

Extended Data Fig. 9 | S and N sensors are functional after lyophilization. a, Both the S and the N sensors can survive lyophilization. The majority of proteins (70–100%) can be reconstituted after lyophilization. The lyophilized S sensors lost 50% of signal. The lyophilized N sensors remain 100% active. **b**, The lyophilized S sensors detected CR3022 at ~50% signal strength compared to fresh sensors. Three technical replicates are plotted from n=1 independent experiment. Lines connecting the means of the samples are plotted. **c**, The lyophilized N sensors detected antibodies from patient sera at similar signal strength compared to fresh sensors. Two technical replicates are plotted from n=1 independent experiment. The bars represent the mean. **d**, Vacuum dried substrate and substrate stored at −20 °C (fresh) behave similarly when detecting recombinant CR3022 with S sensors. Lyophilized dilution buffer and dilution buffer stored at −20 °C (fresh) also showed similar signal. Three technical replicates are plotted from n=1 independent experiment. Lines connecting the means of the samples are plotted.

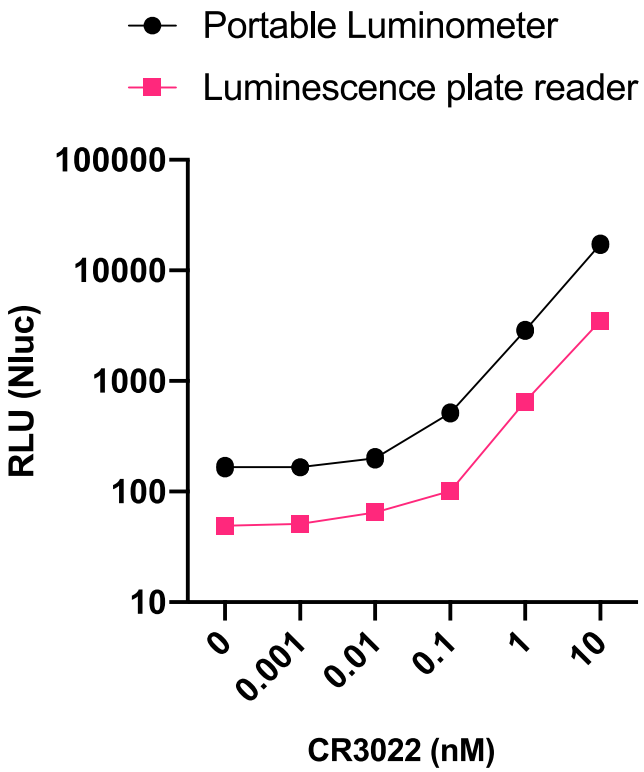

Extended Data Fig. 10 | Portable luminometer. The spLUC assay is also amenable to detection with a Berthold portable luminometer. The handheld luminometer showed similar sensitivity of recombinant CR3022 with S sensors compared to the plate reader. Due to the tube format of the handheld luminometer, the sample volume was doubled and thus the overall signals are higher than for the plate reader samples, but similar sensitivity is maintained. Two technical replicates are plotted from n=1 independent experiment. Lines connecting the means of the samples are plotted.

nature research

Corresponding author(s): James A. Wells

Last updated by author(s): 2/8/2021

Reporting Summary

Nature Research wishes to improve the reproducibility of the work that we publish. This form provides structure for consistency and transparency in reporting. For further information on Nature Research policies, see our Editorial Policies and the Editorial Policy Checklist.

Statistics

For all statistical analyses, confirm that the following items are present in the figure legend, table legend, main text, or Methods section.

n/a	Confirmed	
☐	☒	The exact sample size (*n*) for each experimental group/condition, given as a discrete number and unit of measurement
☐	☒	A statement on whether measurements were taken from distinct samples or whether the same sample was measured repeatedly
☐	☒	The statistical test(s) used AND whether they are one- or two-sided *Only common tests should be described solely by name; describe more complex techniques in the Methods section.*
☒	☐	A description of all covariates tested
☒	☐	A description of any assumptions or corrections, such as tests of normality and adjustment for multiple comparisons
☐	☒	A full description of the statistical parameters including central tendency (e.g. means) or other basic estimates (e.g. regression coefficient) AND variation (e.g. standard deviation) or associated estimates of uncertainty (e.g. confidence intervals)
☐	☒	For null hypothesis testing, the test statistic (e.g. *F*, *t*, *r*) with confidence intervals, effect sizes, degrees of freedom and *P* value noted *Give P values as exact values whenever suitable.*
☒	☐	For Bayesian analysis, information on the choice of priors and Markov chain Monte Carlo settings
☒	☐	For hierarchical and complex designs, identification of the appropriate level for tests and full reporting of outcomes
☒	☐	Estimates of effect sizes (e.g. Cohen's *d*, Pearson's *r*), indicating how they were calculated

Our web collection on statistics for biologists contains articles on many of the points above.

Software and code

Policy information about availability of computer code

Data collection	ForteBio Octet Acquisition software v12; TECAN plate reader software i-control 1.11; NanoDrop 2000c software version 1.6
Data analysis	GraphPad Prism 8.2.1 and Microsoft Excel 16.38 for assay data analysis; Snapgene 3.2.1 and ApE v2.0.47 for cloning design and sequence verification; ForteBio Octet Data analysis software v12; NanoDrop 2000c software version 1.6; PyMOL 2.3.5 for protein structural modeling and analysis; R 4.0.0, Rstudio 1.2.5001, and deSolve package 1.28 for thermodynamic sensor modeling; Thermo Momentum software v5.0.6 for robotic simulation.

For manuscripts utilizing custom algorithms or software that are central to the research but not yet described in published literature, software must be made available to editors and reviewers. We strongly encourage code deposition in a community repository (e.g. GitHub). See the Nature Research guidelines for submitting code & software for further information.

Data

Policy information about availability of data

All manuscripts must include a data availability statement. This statement should provide the following information, where applicable:

- Accession codes, unique identifiers, or web links for publicly available datasets
- A list of figures that have associated raw data
- A description of any restrictions on data availability

The datasets generated during and/or analyzed during the current study are available from the corresponding author J.A.W. on reasonable request. PDB datasets 6XCN, 6W41, 1N8Z, 5IBO, 5D6D used for modeling were downloaded from https://www.rcsb.org/.

Field-specific reporting

Please select the one below that is the best fit for your research. If you are not sure, read the appropriate sections before making your selection.

☒ Life sciences ☐ Behavioural & social sciences ☐ Ecological, evolutionary & environmental sciences

For a reference copy of the document with all sections, see nature.com/documents/nr-reporting-summary-flat.pdf

Life sciences study design

All studies must disclose on these points even when the disclosure is negative.

Sample size	We measured 168 SARS-CoV-2 patient samples and 144 control samples. This sample size is chosen based on the availability of patient samples. It is a sample size that offers sufficient statistical power for calculating assay specificity and sensitivity.
Data exclusions	A few Cohort 1 samples which do not have corresponding patient clinical/demographic information in Robbiani et al, Nature, 584:437, 2020 were excluded and not counted in the 168 samples because the information is needed for the correlation analysis. The exclusion criteria were pre-established.
Replication	All samples were measured at least twice. All attempts at replication were successful.
Randomization	This is not relevant as this is an observational study which do not involve treatment and will not be affected by the relevant bias.
Blinding	Both the samples and the controls were measured in the same samples plates under the same conditions. Data was first processed in blinded mode, followed by sample/control assignments.

Reporting for specific materials, systems and methods

We require information from authors about some types of materials, experimental systems and methods used in many studies. Here, indicate whether each material, system or method listed is relevant to your study. If you are not sure if a list item applies to your research, read the appropriate section before selecting a response.

Materials & experimental systems

n/a	Involved in the study
☐	☒ Antibodies
☐	☒ Eukaryotic cell lines
☒	☐ Palaeontology and archaeology
☒	☐ Animals and other organisms
☐	☒ Human research participants
☒	☐ Clinical data
☒	☐ Dual use research of concern

Methods

n/a	Involved in the study
☒	☐ ChIP-seq
☒	☐ Flow cytometry
☒	☐ MRI-based neuroimaging

Antibodies

Antibodies used	Anti-S protein antibodies C004, C105, C135, CR3022 were recombinantly expressed; the rest of the antibodies were purchased from commercial vendors: anti-N protein antibody (Sino biological, 40588-T62-50); anti-human Fab (Jackson ImmunoResearch Laboratories 109-036-097); anti-human IgM (Sigma-Aldrich A6907), anti-human IgG (Sigma-Aldrich A0170)
Validation	Binding of the C004, C105, C135, CR3022, anti-N antibodies to SARS-CoV-2 S or N proteins were validated using Biolayer interferometry assay and/or the spLUC assay (Fig.1). Based on the manufacture' website, the anti-human Fab antibody was validated by ELISA and immunoelectrophoresis; this antibody reacts with the F(ab')2/Fab portion of human IgG. It also reacts with the light chains of other human immunoglobulins. No antibody was detected against the Fc portion of human IgG or against non-immunoglobulin serum proteins. The antibody has been tested by ELISA and/or solid-phase adsorbed to ensure minimal cross-reaction with bovine, horse and mouse serum proteins, but it may cross-react with immunoglobulins from other species. Based on the manufacture' website, the anti-human IgM and IgG antibodies were validated by ELISA and immunoelectrophoresis. The antibody is specific for human IgG (Fc fragment) when tested against human IgA, IgG (Fab and Fc fragments), IgM, Bence Jones kappa, and lambda myeloma proteins. Cross-reactivity of the antibody-conjugate is determined by ELISA. The conjugate shows no reactivity with mouse or rat IgG. Identity and purity of the antibody is established by immunoelectrophoresis (IEP), prior to conjugation. Electrophoresis of the antibody preparation followed by diffusion versus anti-goat IgG and anti-goat whole serum results in single arcs of precipitation.

Eukaryotic cell lines

Policy information about cell lines

Cell line source(s)	Expi293 (Thermo Fisher) expressing an ER-BirA plasmid (for protein expression only)
Authentication	The cell lines were not authenticated
Mycoplasma contamination	The cell lines were not tested for mycoplasma contamination
Commonly misidentified lines (See ICLAC register)	No commonly misidentified cell lines were used

Human research participants

Policy information about studies involving human research participants

Population characteristics	Cohort 1 patients are consisted of 30 females and 27 males. 26 are within the age bracket of 19-39. 25 are within the age bracket of 40-59; 6 within the age bracket of 60-85. Cohort 3 patients are consisted of 25 females and 31 males. 23 are within the age bracket of 19-39. 25 are within the age bracket of 40-59; 8 within the age bracket of 60-85. No demographic information is available for Cohort 2 patients and controls (and no relevant analysis was performed).
Recruitment	Cohort 1 is an outpatient cohort recruited at the Rockefeller University Hospital. The samples were collected from individuals free of COVID-19 symptoms for >=14 days. Cohort 2 samples are consisted of remnant sera from COVID-19 patients within Kaiser Permanente Hospitals of Northern California. These samples were drawn from hospitalized patients in any phase of infection, including the early acute phase. Little information is available for this group of patients. Cohort 3 patients were part of the LIINC (Long-term Impact of Infection with Novel Coronavirus) study from San Francisco General Hospital and included plasma of a mixture of outpatient and inpatient samples drawn in the convalescent phase of the disease.
Ethics oversight	All patient samples were obtained using protocols approved by the Institutional Review Boards (IRB) and in accordance with the Declaration of Helsinki. Samples were de-identified prior to delivery to the lab where all assays described here were performed. Cohort 1 samples were a kind gift of the Michel Nussenzweig, Marina Caskey, and Christian Gaebler of Rockefeller University, collected with Rockefeller IRB protocol DRO-1006. Cohort 2 samples from Kaiser Permanente were collected with Stanford University IRB protocol #55718. Cohort 3 samples were collected with University of California, San Francisco IRB protocol #20-30479. Influenza virus vaccination samples were from a US cohort enrolled at the Rockefeller University Hospital in New York City in 2012-2013 under a protocol approved by the IRB of Rockefeller University (protocol #TWA-0804). Samples from people with seasonal coronavirus infections were collected at the University of Chicago. Samples were de-identified serums of healthcare workers that had respiratory illnesses, were swabbed, and tested positive for common cold coronavirus infections in 2019 (U. Chicago protocol # 09-043-A).

Note that full information on the approval of the study protocol must also be provided in the manuscript.